

GROUND MOTION SIMULATIONS BASED ON REGIONAL INPUT  
PARAMETERS AND THEIR IMPACT ON INSURANCE PREMIUMS:  
BURSA CASE

A THESIS SUBMITTED TO  
THE GRADUATE SCHOOL OF NATURAL AND APPLIED SCIENCES  
OF  
MIDDLE EAST TECHNICAL UNIVERSITY

BY

BARIŞ ÜNAL

IN PARTIAL FULFILLMENT OF THE REQUIREMENTS  
FOR  
THE DEGREE OF MASTER OF SCIENCE  
IN  
EARTHQUAKE STUDIES

NOVEMBER 2015



Approval of the thesis:

**GROUND MOTION SIMULATIONS BASED ON REGIONAL INPUT  
PARAMETERS AND THEIR IMPACT ON INSURANCE PREMIUMS:  
BURSA CASE**

submitted by **BARIŞ ÜNAL** in partial fulfilment of the requirements for the degree  
of **Master of Science in Earthquake Studies Department, Middle East  
Technical University** by,

Prof. Dr. Gülbin Dural Ünver \_\_\_\_\_  
Dean, Graduate School of **Natural and Applied Sciences**

Assoc. Prof. Dr. Ayşegül Askan Gündoğan \_\_\_\_\_  
Head of Department, **Earthquake Studies**

Assoc. Prof. Dr. Ayşegül Askan Gündoğan \_\_\_\_\_  
Supervisor, **Civil Engineering Dept., METU**

Assoc. Prof. Dr. A. Sevtap Kestel \_\_\_\_\_  
Co-Supervisor, **Institute of Applied Mathematics, METU**

**Examining Committee Members:**

Prof. Dr. Murat Altuğ Erberik \_\_\_\_\_  
Civil Engineering Dept., METU

Assoc. Prof. Dr. Ayşegül Askan Gündoğan \_\_\_\_\_  
Civil Engineering Dept., METU

Assoc. Prof. Dr. A. Sevtap Kestel \_\_\_\_\_  
Institute of Applied Mathematics, METU

Assoc. Prof. Dr. Berna Unutmaz \_\_\_\_\_  
Civil Engineering Dept., HU

Assoc. Prof. Dr. Tolga Yılmaz \_\_\_\_\_  
Engineering Sciencens Dept., METU

**DATE:** 30/11/2015

**I hereby declare that all information in this document has been obtained and presented in accordance with academic rules and ethical conduct. I also declare that, as required by these rules and conduct, I have fully cited and referenced all material and results that are not original to this work.**

Name, Last Name: Barış ÜNAL

Signature:

## ABSTRACT

### GROUND MOTION SIMULATIONS BASED ON REGIONAL INPUT PARAMETERS AND THEIR IMPACT ON INSURANCE PREMIUMS: BURSA CASE

Ünal, Barış

M. S., Department of Earthquake Studies

Supervisor: Assoc. Prof. Dr. Ayşegül Askan Gündoğan

Co-Supervisor: Assoc. Prof. Dr. Sevtap Kestel

November 2015, 95 pages

Ground motion intensity parameters of past and potential earthquakes are required for earthquake resistant design and retrofitting of existing structures. In regions with no or sparse earthquake recordings, most of the available methods generate only peak ground motion parameters. For cases where the full ground motion time histories are required, simulations that consider fault rupture processes become necessary. Simulations can also be used for studying source, path and site effects of past and scenario earthquakes.

In this study, potential earthquakes in Bursa are simulated using stochastic finite-fault simulation method with dynamic corner frequency model. To ensure simulations that yield reliable synthetic ground motions, the input parameters are derived from regional data. Regional model parameters are verified by comparing the records from major previous events in the region against the corresponding

synthetics. Simulation model is also compared with regional and global ground motion prediction equations. Then a potential scenario event with  $M_W = 7.2$  in Bursa is simulated. Spatial distribution of expected peak ground motion parameters and time histories at selected locations are obtained. From these parameters, the corresponding Modified Mercalli Intensities (MMI) are estimated. Later, these MMIs are used as the main ground motion parameter in Damage Probability Matrices (DPM). From the previous seismic hazard studies in the region, the return period of the scenario earthquake is obtained. Finally, insurance rates for Bursa region are determined based on probability of the scenario event and the expected Mean Damage Ratios (MDR) from the corresponding DPMs.

**Keywords:** Ground motion simulation, Stochastic finite-fault model, Insurance premiums, Local seismic parameters

## ÖZ

### YEREL VERİLERLE YER HAREKETİ SİMÜLASYONU VE BU VERİLERİN SİGORTA PRİMLERİNE ETKİSİ: BURSA ÖRNEĞİ

Ünal, Barış

Yüksek Lisans, Deprem Çalışmaları Bölümü

Tez Yöneticisi: Doç. Dr. Ayşegül Askan Gündoğan

Yardımcı Tez Yöneticisi: Doç. Dr. Sevtap Kestel

Kasım 2015, 95 sayfa

Depreme karşı dayanıklı yapıların tasarımında ve eski binaların güçlendirme projelerinde deprem parametrelerine ihtiyaç duyulmaktadır. Deprem kaydı olmayan ya da çok az olan bölgelerde kullanılabilen yöntemlerden, çoğu zaman yalnızca maksimum yer hareketi parametreleri elde edilebilmektedir. İvme-zaman grafiğine ihtiyaç duyulan durumlarda fayın kırılma sürecini hesaba katan simülasyonlara ihtiyaç duyulmaktadır. Simülasyonlar ayrıca geçmiş depremlerin veya potansiyel senaryo depremlerinin kaynak, yayılım ve saha etkileri hakkında bilgi edinmek içinde kullanılabilir.

Bu çalışmada Bursa bölgesinde meydana gelme olasılığı olan potansiyel depremlerin dinamik sınır frekanslı stokastik sonlu-fay simülasyon modeli ile simülasyonları yapılmıştır. Simülasyonların güvenilir yer hareketi sonuçları vermesi için girdi parametreleri yerel verilerden elde edilmiştir. Bölgede daha önce meydana gelen depreme ait yer hareketleri ile bu depremlerin simülasyon sonuçları

karşılaştırılmış, simülasyon modeli doğrulanmıştır. Simülasyon modeli ayrıca yerel ve global azalım denklemleri ile de karşılaştırılmıştır. Daha sonra Bursa'da  $M_W = 7.2$  büyüklüğünde potansiyel bir deprem senaryosunun simülasyonu yapılmıştır. Seçilen noktalarda bu senaryo depreminin oluşturduğu maksimum yer ivmeleri hesaplanıp mekansal dağılımları elde edilmiştir. Maksimum yer ivmelerinden depremin o noktadaki Modified Mercalli Intensity (MMI) cinsinden şiddeti bulunmuştur. Deprem şiddet parametresi Hasar Olasılık Matrislerinde (HOM) kullanılarak ana girdi parametresi olarak kullanılmıştır. Bölgede daha önce yapılmış olan sismik tehlike analizlerinden senaryo depreminin tekrarlanma periyodu elde edilmiştir. Son olarak hasar olasılık matrislerinden elde edilen ortalama hasar oranlarından ve senaryonun tekrarlanma periyodundan Bursa bölgesi için sigorta primleri hesaplanmıştır.

**Anahtar kelimeler:** Yer hareketi simülasyonu, Stokastik sonlu fay modeli, Sigorta primleri, Yerel sismik parametreler

To my friends, my advisors and my family

## ACKNOWLEDGMENTS

I would like to express my gratitude to Assoc. Prof. Dr. Ayşegül Askan Gündoğan. Her knowledge and optimism guided this study into the right path. Her selfless efforts are truly appreciated. Her recommendations, trust and highly motivated stance were impactful not only on this study but also for me as a researcher.

I would like to thank Assoc. Prof. Dr. Sevtap Kestel for her patience and valuable suggestions. With her guidance this study is enhanced and became a multi-disciplinary work.

I am grateful to Dr. Nazan Kılıç for her selfless efforts. Her reviews and input on the Bursa scenario earthquake are deeply appreciated.

I would like to thank Shaghayegh Naghshineh and Mustafa Bilal for their support on the GIS part of this study. I would also like to thank Fatma Nurten Şişman for her guidance on kappa factor calculations.

I am grateful to Uğurcan Özçamur and Gizem Can for offering their help anytime I needed and encouraging me to keep going.

I would like to thank teammates from A-Team; Aida Azari Sisi , Saideh, Shaghayegh Naghshineh, Fatma Nurten Şişman and Gizem Can. Their support and team events will always be remembered.

I would also like to thank my lunch time companions Uğurcan Özçamur, Sanem Elidemir and Çidem Argünhan. Without their support my masters study would not be as joyful.

## TABLE OF CONTENTS

ABSTRACT .....	v
ÖZ.....	vii
ACKNOWLEDGMENTS.....	x
TABLE OF CONTENTS .....	xi
LIST OF TABLES .....	xiv
LIST OF FIGURES.....	xvi
CHAPTERS	
1 INTRODUCTION.....	1
1.1 General.....	1
1.2 Literature Survey .....	2
1.3 Objective and Scope .....	4
2 STOCHASTIC STRONG GROUND MOTION SIMULATION METHODOLOGY .....	7
2.1 General.....	7
2.2 Stochastic Point Source Modeling.....	7
2.2.1 Source Effects .....	10
2.2.2 Path Effects .....	13
2.2.3 Site Effects .....	15

2.2.3.1	Amplification Function .....	16
2.2.3.2	Diminution Function .....	17
2.3	Stochastic Finite-Fault Modeling .....	19
3	GROUND MOTION SIMULATIONS IN BURSA REGION .....	25
3.1	General.....	25
3.2	Background information .....	25
3.3	Strong Ground Motion Dataset.....	26
3.4	Model Parameters .....	30
3.4.1	Source parameters .....	31
3.4.2	Path parameters .....	32
3.4.3	Site parameters .....	33
3.5	Optimization for Model Parameters .....	41
3.6	Simulation Results .....	44
3.6.1	Comparison of Simulated and Observed Data .....	44
3.7	Comparison of Synthetics and Ground Motion Prediction Equations and Observations.....	49
4	SCENARIO EARTHQUAKE ON BURSA FAULT AND INSURANCE IMPLICATIONS.....	53
4.1.	Components of Earthquake Insurance .....	53

4.2.	Bursa Fault Scenario.....	54
4.3.	Earthquake Insurance Practice.....	57
4.4.	Damage Probability Matrices for Turkey .....	59
4.5.	Valuation of the Earthquake Insurance Premium.....	62
4.6.	Comparison of the Premium Calculation Methods .....	67
5	CONCLUDING REMARKS .....	69
5.1	Summary.....	69
5.2	Observations and Conclusions .....	70
5.3	Future Recommendations .....	711
	REFERENCES.....	75
	APPENDICES	
	A $\kappa_0$ VALUES FOR BURSA STATIONS .....	83
	B BOREHOLE LOGS OF STATIONS 1610, 1611, 1612 AND 1614 .....	85
	C CORRELATIONS OF SEISMIC VELOCITIES WITH GEOTECHNICAL BOREHOLE DATA AT STATIONS 1610, 1611, 1612 AND 1614 .....	93

## LIST OF TABLES

### TABLES

Table 3.1 Selected earthquakes near Bursa City .....	27
Table 3.2 Information on stations that recorded Bilecik earthquake .....	29
Table 3.3 Information on stations that recorded Karacabey earthquake .....	29
Table 3.4 Information on stations that recorded Keles earthquake .....	30
Table 3.5 Information on stations that recorded M.Kemalpasa earthquake.....	30
Table 3.6 Parameters used for verification simulations .....	43
Table 4.1 Parameter set utilized for Bursa scenario earthquake .....	55
Table 4.2 Yearly premium number and total premium values (TCIP, 2015) .....	58
Table 4.3 Earthquake insurance premium rates for Turkey (TCIP, 2015).....	59
Table 4.4 Central damage ratios for damage states Gurpinar et al. (1978).....	60
Table 4.5 Damage probability matrix proposed by Gurpinar et al. (1978).....	61
Table 4.6 Damage probability matrix for Zone 1 (Askan and Yucemen, 2010)....	62
Table 4.7 Pure risk premiums calculated from Askan and Yucemen (2010) DPM63	
Table 4.8 Modified DPM with respect to loss level method.....	64

Table 4.9 Pure risk premiums with respect to loss level method.....	65
Table 4.10 DPM generated from damage simulations.....	66
Table 4.11 Pure risk premium calculated by using the DPM generated from damage simulations .....	66
Table 4.12 Comparison of pure premiums with respect to three models.....	67
Table 4.13 Gross premium with respect to three models.....	68
Table A.1 $\kappa_0$ Values for Bursa Stations .....	83

## LIST OF FIGURES

### FIGURES

Figure 2.1 Flowchart of the stochastic point-source method .....	10
Figure 2.2 Wave propagation on a rectangular finite-fault model .....	20
Figure 3.1 Major faults near Bursa Region. ....	26
Figure 3.2 Location of the epicenters of the selected earthquakes and the recording stations.....	28
Figure 3.3 Site amplification from alternative techniques at station a)1603, b)1605, c)1606, d)1607, e)1608 and f)1609 .....	35
Figure 3.4 Site amplification from alternative techniques at station 1610 b) Modified Vs profile of Station 1610 .....	36
Figure 3.5 Site amplification from alternative techniques at station 1611 b) Modified Vs profile of Station 1611 .....	36
Figure 3.6 Site amplification from alternative techniques at station 1612 b) Modified Vs profile of Station 1612 .....	36
Figure 3.7 Site amplification from alternative techniques at station 1613.....	37
Figure 3.8 Site amplification from alternative techniques at station 1614 b) Modified Vs profile of Station 1614 .....	37
Figure 3.9 Site amplification from alternative techniques at station a)1615 and b)1618.....	37

Figure 3.10 Horizontal kappa model of station a)1603 and b)1605.....	39
Figure 3.11 Horizontal kappa model of station a)1606, b)1607, c)1608, d)1609, e)1613 and f)1615 .....	40
Figure 3.12 Horizontal kappa model of station 1618.....	41
Figure 3.13 Quality factor options for parameter optimization .....	42
Figure 3.14 Comparison of Observed and Simulated Records for Bilecik Earthquake .....	44
Figure 3.15 Comparison of Observed and Simulated Records for Karacabey Earthquake.....	46
Figure 3.16 Comparison of Observed and Simulated Records for Keles Earthquake .....	47
Figure 3.17 Comparison of Observed and Simulated Records for M.Kemalpaşa Earthquake.....	48
Figure 3.18 GMPE comparisons for $M_w=5$ .....	50
Figure 3.19 GMPE comparisons for $M_w=5.5$ .....	50
Figure 3.20 GMPE comparisons for $M_w=6$ .....	51
Figure 3.21 GMPE comparisons for $M_w=6.5$ .....	51
Figure 3.22 GMPE comparisons for $M_w=7$ .....	52
Figure 4.1 Peak ground acceleration distribution around Bursa City for $M_w=7.2$ scenario earthquake .....	56

Figure 4.2 Distribution of MMI corresponding to the $M_w=7.2$ scenario earthquake around Bursa City.....	57
Figure B.1 Borehole log of station 1610 part 1 .....	85
Figure B.2 Borehole log of station 1610 part 2.....	86
Figure B.3 Borehole log of station 1611 part 1 .....	87
Figure B.4 Borehole log of station 1611 part 2.....	88
Figure B.5 Borehole log of station 1611 part 3.....	88
Figure B.6 Borehole log of station 1612 part 1 .....	89
Figure B.7 Borehole log of station 1612 part 2.....	90
Figure B.8 Borehole log of station 1612 part 3.....	90
Figure B.9 Borehole log of station 1614 part 1 .....	91
Figure B.10 Borehole log of station 1614 part 2.....	92
Figure C.1 Correlations of seismic velocities with geotechnical borehole data at station 1610 .....	93
Figure C.2 Correlations of seismic velocities with geotechnical borehole data at station 1611 .....	94
Figure C.3 Correlations of seismic velocities with geotechnical borehole data at station 1612 .....	94
Figure C.4 Correlations of seismic velocities with geotechnical borehole data at station 1614 .....	95

## **CHAPTER 1**

### **INTRODUCTION**

#### **1.1 General**

Earthquakes are among the most catastrophic natural hazards. Apart from economic losses and destruction of structures, these events also have devastating social and psychological effects on the society. Considering the rate of occurrence and the unpredictable nature combined with their damage potential, studying earthquakes are crucial. Earthquake studies involve multiple research areas from earth sciences to social sciences; from structural engineering to insurance industry.

For reliable seismic design, restoration and retrofitting of buildings; estimation of seismic loads is fundamental. For an accurate estimation of these loads, ground motion parameters such as amplitude, frequency content and duration are necessary. The best option for gathering these information is to use regional real ground motion records. However, this requires that the region is monitored extensively for a long period of time. Thus, obtaining real ground motion records from past events is especially difficult for regions with sparse or no seismic networks. Another option is to get records from a region similar to the study area in terms of tectonics and site conditions. However, finding two sites with identical or very similar physical properties is very difficult.

Ground Motion Prediction Equations (GMPEs) -formerly known as attenuation relationships- are mathematical tools that fit parametric models to past records in

order to predict future data. GMPEs are frequently used for engineering purposes. However, regional GMPEs can suffer from lack of accuracy since they generally have incomplete data set, especially for large magnitude events at short distances. Global GMPEs, on the other hand, are derived from larger data sets, thus the regional characteristics may not be represented sufficiently. Moreover, these equations still contain large uncertainties as the number of large magnitude events is small even in the global scale. Finally, GMPEs do not provide the full time histories but only the peak ground motion parameters. Therefore, ground motion simulations become a significant alternative for obtaining strong ground motion time histories. Recent GMPEs also utilize ground motion simulations for large magnitude earthquakes in order to supplement their data sets (Chiou and Youngs, 2014).

Ground motion simulations have two major solution approaches: Deterministic and stochastic solutions. In deterministic simulations, full wave propagation is solved analytically or numerically. With a well-refined wave velocity model these simulations yield the most physical representation of ground motions. However, these methods require excessive computational power and very dense information on earth material properties at higher frequencies. This limits the high frequency bound of the deterministic simulations. On the other hand, stochastic methods are very powerful at modeling intermediate and high frequencies but these methods are less accurate for not solving the full wave propagation. The best option for obtaining a realistic broadband record is to use hybrid methods. These methods utilize deterministic approach for low frequencies and stochastic approach for intermediate and higher frequencies, respectively. Since the building structures are mostly affected by intermediate and higher frequencies, stochastic methods are viable for engineering purposes. Due to this observation in addition to lack of velocity models in the study region, stochastic approach is employed in this thesis.

## **1.2 Literature Survey**

Ground motion simulations are studied mostly by earth scientists and earthquake engineers. Earth scientists generally utilize ground motion simulations to understand

fault mechanisms and investigate path and site effects. Earthquake engineers use these simulations for obtaining peak ground motion parameters, frequency content and full time history of a past or potential earthquake for a region with sparse seismic recordings.

As deterministic ground motion simulations are limited to low frequencies, stochastic approach is developed in order to simulate intermediate and higher frequencies. Stochastic approach was first developed as superimposing impulses that have random amplitudes and durations with random time intervals (Housner, 1947; Housner, 1955; Thomson, 1959). Later, Aki (1967) improved the source model by modeling displacement as a ramp function of time, and showed that the source spectrum decreases proportional to the square of frequency ( $\omega^{-2}$ ). This model was then found to be the best physical representation of earthquakes (Brune, 1970; Hanks, 1979). Brune (1970, 1971) further improved the source model proposed by Aki (1967) by estimating the source-time function from the effective stress available near the fault plane. Hanks and McGuire (1981) showed that the randomness in the high frequency portion of the source spectrum can be modeled with white Gaussian noise.

Boore (1983) later combined the source spectrum of Aki (1967) and Brune (1971) with the findings of Hanks and McGuire (1981) and proposed a methodology for generating time-domain simulations of ground motion records. In this method, faults are modeled as stochastic point sources. Beresnev and Atkinson (1997) modified this model for near-fault effects. In their model, faults are divided into finite subfaults. Each subfault is represented as a stochastic point source. They combined the effects of these subfaults to obtain overall effect of the ground motion. Motazedian and Atkinson (2005) further improved the stochastic finite-fault modeling by introducing the dynamic corner frequency approach. In the static corner frequency approach, modeling the same ground motion with different subfault lengths results in different amplitudes. In the dynamic corner frequency approach, the corner frequency decreases inversely proportional to the ruptured area while the rupture propagates. This results in amplitudes independent of the chosen subfault dimensions.

Stochastic ground motion simulation method is validated in various studies for California region by Hanks and Boore (1984) Atkinson and Silva (2000), Motazedian and Atkinson (2005). Similar validation studies were performed in Italy (Castro et al., 2001; Castro et al., 2008; Galluzzo et al., 2008; Ugurhan et al. 2012); Greece (Roumelioti et al., 2004); Iran (Motazedian and Moinfar, 2006; Shoja-Taheri and Ghofrani, 2007) and in India (Raghukanth and Somala, 2009). Stochastic method is also validated in several studies in Turkey for the 1998 Ceyhan (Yalcinkaya, 2005), 1999 Düzce (Ugurhan and Askan, 2010) and 1992 Erzincan (Askan et al., 2013), 2011 Van (Akinci and Antonioli, 2013; Zengin and Cakti, 2014) earthquakes.

In this study, stochastic finite-fault simulation method with dynamic corner frequency as developed by Motazedian and Atkinson (2005) is utilized for Bursa region.

### **1.3 Objective and Scope**

In this thesis, past events and potential scenario earthquakes in Bursa are simulated using stochastic finite-fault simulation approach with dynamic corner frequency model. The main objective of this thesis is to obtain ground motion parameters for a potential earthquake in this region and to calculate insurance premiums for this scenario earthquake. For this purpose, initially regional source, path and site parameters are investigated. Major past earthquakes are then simulated with these regional parameters to verify the simulation model. After the verification of the model, a potential scenario earthquake is simulated to assess the anticipated peak ground motion parameters in the Bursa region. Next, these parameters are converted to structural damage ratios using Damage Probability Matrices (DPMs). From the expected damage ratio and the probability of the studied scenario event, insurance premiums are calculated.

In Chapter 2, the underlying theory behind the stochastic finite-fault method is presented. Progression of the theory from stochastic point-source method to stochastic finite-fault method with dynamic corner frequency approach is discussed. Parameters required in this approach are described in detail.

In Chapter 3, Bursa region is studied. Initially, background information on the seismic and tectonic properties of the region is given. Then, real ground motion data used in the ground motion simulations are introduced. Estimation and optimization of the model parameters are discussed next. Finally, ground motion simulations are performed and results are compared against the observed records as well as ground motion prediction equations (GMPEs).

In Chapter 4, first, through the seismic hazard assessment studies in the literature, a potential scenario earthquake for Bursa region is selected. Using the verified model parameters defined in Chapter 3, this event is simulated. From these simulations, the spatial distribution of the anticipated ground motion parameters are obtained. These parameters are then transformed into structural damage ratios using damage probability matrices. Finally, from the expected damage ratio and the probability of this scenario event, insurance premiums in Bursa region are calculated. Three alternative models are used to compute insurance premiums. The results are compared with each other.

Chapter 5 summarizes the main findings of the thesis and concludes this study. Main observations are discussed and future recommendations are presented.



## **CHAPTER 2**

### **STOCHASTIC STRONG GROUND MOTION SIMULATION METHODOLOGY**

#### **2.1 General**

In this chapter, the fundamentals of the stochastic strong ground motion simulation methodology are described. In section 2.2 the theory behind stochastic point source simulation method is explained. In this method, models for source effects, path effects and site conditions are combined with windowed Gaussian noise in frequency domain to obtain simulated far field acceleration time history. In subsections 2.2.1, 2.2.2 and 2.2.3 source, path and site parameters are presented in detail, respectively. In section 2.3 stochastic finite-fault simulation method is described. Advantages of this method for simulating near-fault records along with differences from the point source models are presented. Finally, static and dynamic corner frequency approaches are explained.

#### **2.2 Stochastic Point Source Modeling**

In earthquake engineering, high frequency portion of strong ground motions, particularly of S-waves, are critical for damage potential. Unless there are well-defined high-resolution velocity models in the study areas, numerical solutions of seismic wave propagation equation become inefficient after  $f > 1$  Hz. In addition,

complex phase characteristics of high frequencies require models for randomness in ground motion simulations. Through the use of random phase angles and modeling in frequency domain, stochastic methods greatly reduce the computational efforts. It is also well known that the stochastically-simulated motions predict peak ground motion parameters, full acceleration time series and Fourier Amplitude Spectrum (FAS) with reasonable accuracy (Hanks and McGuire, 1981; Boore, 1983; Silva and Lee, 1987; Toro and McGuire, 1987).

Stochastic modeling has two main parts; deterministic amplitude spectra obtained from Green's function solution of the elastic wave propagation equation and a stochastic time series. A windowed stochastic time series is scaled in the frequency domain such that its amplitude is almost equal to that of the deterministic target spectra. The  $\omega^2$  spectrum with a high-frequency cut-off as proposed by Aki (1967) greatly improved the accuracy of the estimated peak ground acceleration (Hanks and McGuire, 1981).

Following the findings of Hanks and McGuire (1981) that high-frequency ground motion of shear-waves can be represented as finite duration, band-limited, white Gaussian noise; Boore (1983) introduced a method for generating S-wave portion of the seismic waves due to point-sources. The objective of this simulation method is to obtain a transient time series whose amplitude spectrum matches the theoretical deterministic spectrum on the average. In this method, amplitude spectrum of filtered and windowed Gaussian white noise approximated to an acceleration spectrum obtained by removing frequencies above a certain cut-off frequency of Brune (1970) spectrum while considering physical aspects of the fault rupture. The model is scaled with earthquake size depending on only the seismic moment of the earthquake. This method is implemented with an only one stress parameter: stress drop. This simple approach provided good approximations to high frequency portion of many past strong ground motion recordings.

The first part of stochastic ground motion simulation method is generating random band-limited Gaussian white noise with zero mean and unit variance. To obtain a more realistic acceleration time history, this time series is windowed with Saragoni-

Hart Window (Saragoni and Hart, 1973). Then this noise is normalized by the square root of the mean squared amplitude spectrum in the frequency domain. Finally, this normalized spectrum is multiplied with the deterministic target S-wave spectrum. Transforming the series back into time domain yields stochastic acceleration-time series (Boore, 2003). The algorithm is shown in Figure 2.1. The product of filter functions representing the source (E), propagation (P), site effects (G), and the instrument response (I), results in the Fourier Amplitude Spectrum of a seismic signal given as:

$$A(M_0, R, w) = E(M_0, w)P(R, w)G(w)I(w) \quad (2.1)$$

where  $M_0$  is the seismic moment,  $w$  is the frequency,  $R$  is the source to site distance.

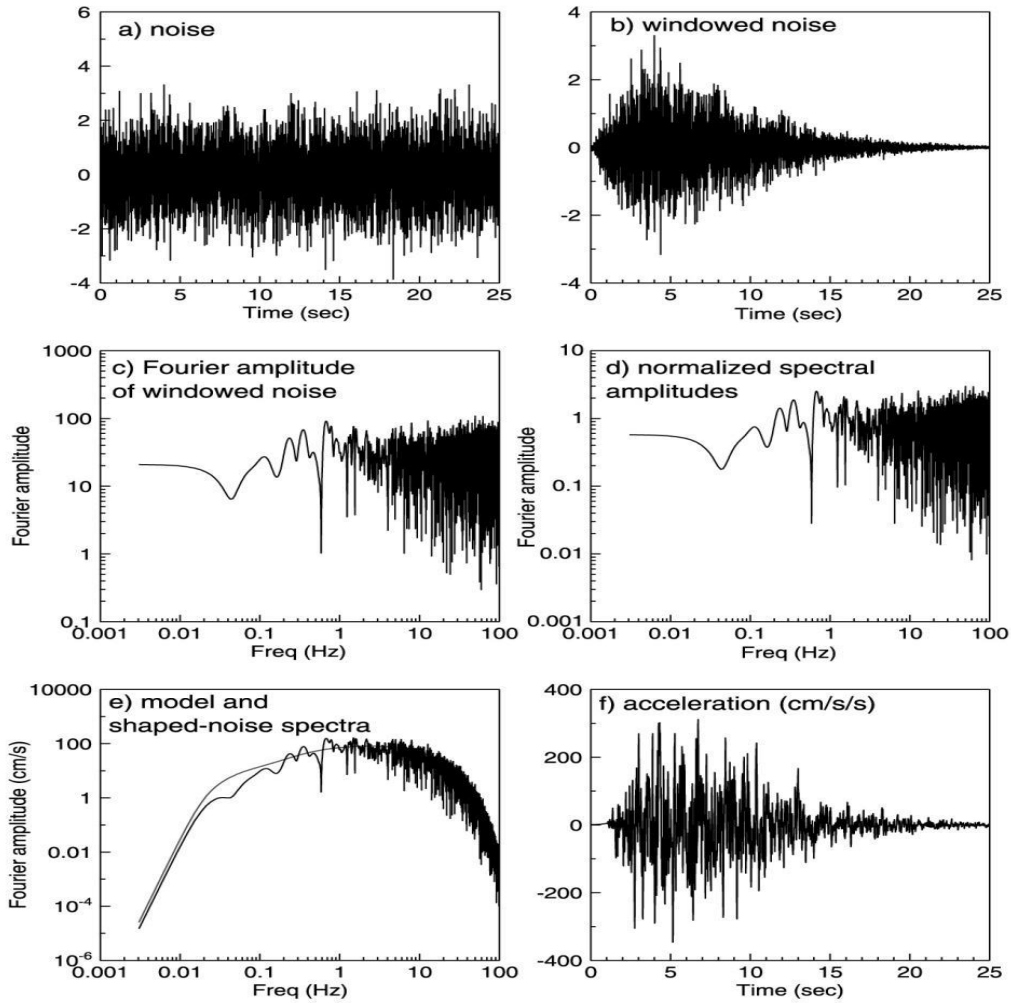


Figure 2.1 Flowchart of the stochastic point-source method (adapted from Boore, 2003)

### 2.2.1 Source Effects

Source effects are basically expressed as filter functions in terms of earthquake size, shear modulus of the earth material at the fault depth and the source time function. These functions affect shape and amplitude of the resulting spectrum. For the earthquake source spectrum, Aki's (1967)  $\omega^2$  model is used.

To define the source spectrum, initially Green's function solution for the far-field shear wave displacement in a homogeneous, isotropic, unbounded medium due to a point shear dislocation is expressed in time domain as follows:

$$u(x, t) = \frac{\mathfrak{R}^{\theta\gamma}}{4\pi\rho\beta^3R} M'(t) \left( t - \frac{R}{\beta} \right) \quad (2.2)$$

where  $u(x, t)$  is the dynamic displacement field at point  $x$ ,  $\mathfrak{R}^{\theta\gamma}$  is the radiation pattern reflecting the variation of the displacement field for different directions due to a shear dislocation,  $\beta$  is the shear-wave velocity,  $R$  is the source to receiver distance and  $M'(t)$  is the moment rate function which is the time derivative of the seismic moment  $M(t)$  (Aki and Richards, 1980).

Seismic moment is defined as:

$$M(t) = \mu \bar{u}(t) A \quad (2.3)$$

where  $\mu$  is the shear modulus or rigidity,  $\bar{u}(t)$  is the source time function and  $A$  is the dislocation area.

Source time function inherits major uncertainty. Aki (1967) utilized a step function to represent the increase of particle displacement with time while Haskell (1964) assumed a ramp function. The source-time function used in stochastic modeling belongs to Brune (1970) where the dislocation is modeled as a function of the effective stress that accelerates the sides of the fault. It is modified by Beresnev and Atkinson (1997) to satisfy the boundary conditions.

The source time function used in stochastic modeling is:

$$\bar{u}(t) = \frac{\sigma}{\mu} \beta \tau \left[ 1 - \left( 1 + \frac{t}{\tau} \right) e^{-\frac{t}{\tau}} \right] \quad (2.4)$$

while the velocity is:

$$\bar{u}'(t) = \frac{\sigma}{\mu} \beta \left( \frac{t}{\tau} \right) \left( e^{-\frac{t}{\tau}} \right) \quad (2.5)$$

Thus, Equation (2.2) is rewritten as:

$$u(x, t) = \frac{\Re^{\theta\gamma} M_0}{4\pi\rho\beta^3 R\tau} \left( \frac{t - \frac{R}{\beta}}{\tau} \right) e^{-\frac{[t - \frac{R}{\beta}]}{\tau}} \quad (2.6)$$

Fourier transformation of Equation (2.6) is:

$$u(x, \omega) = \frac{\Re^{\theta\gamma} M_0}{4\pi\rho\beta^3 R} \left[ \frac{1}{1 + \left( \frac{\omega}{\omega_c} \right)^2} \right] \quad (2.7)$$

Here the corner frequency ( $f_c = \omega_c/2\pi$ ) is defined by Brune (1970, 1971) as:

$$f_c = 4.9 \times 10^6 \beta \left( \frac{\Delta\sigma}{M_0} \right)^{1/3} \quad (2.8)$$

where  $f_c$  is expressed in Hertz (Hz), shear-wave velocity  $\beta$  in km/sec, stress drop  $\Delta\sigma$  in bars and the seismic moment  $M_0$  in dyne-cm.

To summarize, the general form of the source function in terms of constants C, seismic moment and source displacement spectrum is expressed as follows:

$$E(M_0, \omega) = CM_0S(\omega, \omega_c) \quad (2.9)$$

where  $C$  is the combined form of the constants as follows:

$$C = \frac{\mathfrak{R}^{\theta\gamma} \cdot FS \cdot PRTITN}{4\pi\rho\beta^3} \quad (2.10)$$

Here,  $FS$  is the free surface amplification factor whose value is generally assumed to be 2.  $PRTITN$  is a factor applied to reflect the effect of shear-wave energy partitioning into two horizontal components and its value is taken to be  $1/\sqrt{2}$ . The radiation pattern constant  $\mathfrak{R}^{\theta\gamma}$  is mostly taken as 0.55 for shear waves.

Finally, based on the previous derivations, the source displacement spectrum ( $\omega^{-2}$  spectrum) is defined as:

$$S(\omega, \omega_c) = \frac{1}{1 + \left(\frac{\omega}{\omega_c}\right)^2} \quad (2.11)$$

The major limitation of stochastic ground motion models is the source models. Complex source behavior regarding fault rupture is not fully defined in the source processes. For this reason, stochastic models are observed to work only limitedly for the lower frequencies which are most affected from the source effects during large earthquakes (Askan et al., 2013). However, for most residential structures the low frequencies are not critical. Therefore simulated ground motions with stochastic approach are considered to be useful for earthquake engineering purposes.

### 2.2.2 Path Effects

As seismic waves travel through deeper layers of the earth, their amplitude, frequency content and the duration are modified. These effects are modeled by the

path parameters which include geometric spreading, quality factor (anelastic attenuation factor) and duration functions.

Intensity of waves diminishes as they travel further away from their source. Seismic waves also obey this rule. However, since the earth is not a homogeneous body, the geometric spreading term is not simply  $1/R$  where  $R$  is the distance from the source. Instead, the geometric spreading term is derived from regional or global datasets. Boore (2013) used the following piecewise continuous geometric spreading function:

$$Z(R) = \left\{ \begin{array}{ll} \frac{R_0}{R}, & R \leq R_1 \\ Z(R_1) \left(\frac{R_1}{R}\right)^{p_1}, & R_1 \leq R \leq R_2 \\ \vdots \\ Z(R_n) \left(\frac{R_n}{R}\right)^{p_n}, & R \leq R_n \end{array} \right\} \quad (2.12)$$

Since the Earth is not completely elastic, seismic waves are subjected to damping. This is the second reason for the amplitude diminution of seismic waves while traveling through the Earth. This anelastic attenuation is expressed in terms of quality factor function and represented as:

$$Q(f) = Q_0 f^n \quad (2.13)$$

where  $Q_0$  is related to heterogeneous behavior of Earth media and  $n$  is a region-dependent parameter (Raghukanth and Somala, 2009). Quality factor is frequency-dependent especially at higher frequencies. As the quality factor decreases damping increases and waves attenuate faster. This attenuation factor is modeled in stochastic ground motion modeling method with the filter function  $e^{-\frac{\pi f R}{Q(f)\beta}}$ .

This anelastic attenuation is region-specific; therefore it must be derived from regional seismic data. However, since source and path effects are ambiguous and the inversion problem is non-unique mathematically, there may be different models for the same region. In such cases, simulations with the best model reveal the closest fit to the recorded data.

In summary, the frequency-dependent path effects in stochastic ground motion simulations are modeled as:

$$P(R, w) = Z(R)e^{-\frac{\pi f R}{Q(f)\beta}} \quad (2.14)$$

Distance-related duration is not included in the deterministic target spectrum. Yet, for the time history representation of the simulated signal, a duration function is required. The form of the duration function is given as:

$$T = T_0 + bR_{hypo} \quad (2.15)$$

where  $T_0$  the source duration and  $b$  is the slope of distance-dependent duration term where  $R$  is the source to site distance (Beresnev and Atkinson, 1997).

### 2.2.3 Site Effects

Soil profile underneath any site of interest affects the amplification and diminution of the strong ground motion waves. These local site effects depend on the reflection and refraction processes within the heterogeneous Earth structure beneath the sites. In most cases, for simplicity Earth is modeled as a one-dimensional layered system. Therefore soil type, layer thickness and wave velocity parameters are important for the accurate modeling of the site effects.

Site conditions affect the frequency content, amplitude and duration of the seismic waves. Generally, the density and velocity of soils decrease from bedrock to the surface. Accordingly, the seismic impedance decreases when waves travel up

through the Earth. Thus, wave amplitudes must increase in order to conserve the elastic wave energy (Kramer, 1996). On the other hand, softer soils cause damping on the seismic waves which has a decreasing effect on the amplitude. Therefore site models must include both amplification and diminution effects. In stochastic ground motion simulations, the complete site effects filter is represented as:

$$G(f) = A(f)D(f) \quad (2.16)$$

where  $A(f)$  is the amplification and  $D(f)$  is the diminution function.

### **2.2.3.1 Amplification Function**

There are several methods for determining the site amplification factors. Among these methods, the most accurate one is the theoretical method which requires the velocity profile to be known in detail. Velocity profiles are generally obtained from expensive and difficult in-situ procedures. Thus, empirical methods can be preferred for some sites.

When the velocity profile is known, for estimating site amplifications 1-D theoretical site response analyses are generally preferred (Schnabel et al., 1972). In this method, the site is modeled with infinite horizontal soil layers resting on a uniform half space as an equivalent linear system. Theoretical transfer function is obtained from solution of 1-D wave propagation through these soil layers. For more complex problems like modeling basin effects, 2-D or 3-D velocity models are used (e.g.: Sanchez-Sesma, 1987; Pitarka et al., 1998).

Another theoretical method is quarter wavelength approach. In this approach, the amplification corresponding to some particular frequency is given by the square root of the ratio of the seismic impedance corresponding to the depth of source to the average seismic impedance calculated over a depth corresponding to a quarter of wavelength (Boore and Joyner, 1997) as follows:

$$A(f(z)) = \sqrt{\frac{\rho_s \beta_s}{\rho(z) \bar{\beta}(z)}} \quad (2.17)$$

where  $f(z) = 1/[4 \times S_{tt}(z)]$  frequency corresponding to depth  $z$  where  $S_{tt}(z)$  is the  $S$  travel time from the surface to depth  $z$ .  $\rho(z)$  is the density at depth  $z$ .  $\bar{\beta}(z) = z/S_{tt}(z)$  is the average velocity at depth  $z$ . And the subscript  $s$  represents the values in the vicinity of the source.

These amplifications are calculated for NEHRP soil classes by Boore and Joyner (1997). Thus, without detailed information about the soil profile, with only NEHRP class of the site, site amplification can be estimated with this generic amplification functions.

As an alternative to the theoretical approaches, Nakamura (1989) proposed an empirical method (Horizontal-to-Vertical spectral ratio, H/V) for obtaining site amplifications when velocity profile of the site is unknown. This method is based on the assumption that the vertical component of the seismic waves is not exposed to the site effects as much as the horizontal components. However, both vertical and horizontal components are influenced by the same path and source effects. Therefore, dividing the horizontal components to the vertical component should eliminate the source and path effects. One of the main benefits of this method is that weak ground motions and aftershocks can be used to get an estimate of the fundamental frequencies and the corresponding amplifications. Yet, when utilized with incomplete data sets, this method is generally subjected to large uncertainties.

### 2.2.3.2 Diminution Function

Under the effect of near-field conditions, a rapid decay of the spectral values in the high-frequencies is observed. This diminution effect is not due to the attenuation during wave propagation (Boore, 1983). There are different opinions about where this decay should be attributed. Papageorgiou and Aki (1983) suggest that this loss

is caused by the source processes, whereas Hanks (1982) and Atkinson (2004) point out that this decay is related to the near-surface site conditions.

There are two well-known methods for modeling this decay at frequencies above a cut-off frequency. The first approach is the  $f_{\max}$  filter (Hanks, 1982), where the diminution function becomes:

$$D(f) = \left( 1 + \left( \frac{f}{f_{\max}} \right)^8 \right)^{-0.5} \quad (2.18)$$

Here  $f_{\max}$  is the cut-off frequency.

Second approach is the use of the “kappa operator” introduced by Anderson and Hough (1984). Anderson and Hough (1984) modeled the spectral decay at higher frequencies as an exponential function. In this approach, kappa parameter can be computed for both horizontal and vertical components. First, Fourier acceleration spectrum of the record is plotted in semi-logarithmic scale. A best fit line to the decaying portion is obtained manually. Dividing the slope of the best fit line to  $-\pi$ , the kappa values for the record is obtained. However, this kappa value inherits the effects of the path between hypocenter and station. Therefore, a zero-distance kappa value ( $\kappa_0$ ) is used for the calculation of the site effects. In order to determine the  $\kappa_0$  value, individual kappa values of various recordings recorded at the region or site of interest are plotted against epicentral distances of these records. Ordinate, the value at epicentral distance is equal to zero, of the best fit line is the  $\kappa_0$  value. The corresponding filter function in stochastic modeling is defined as:

$$D(f) = e^{-\pi\kappa_0 f} \quad (2.19)$$

## 2.3 Stochastic Finite-Fault Modeling

Stochastic point source modeling is valid for sites that are located at greater distance than the causative fault's largest dimension. For near-fault sites however, the dimensions and orientation of the fault becomes significant due to the near-fault effects observed in the recorded ground motions. Beresnev and Atkinson (1997) approached this problem by dividing the fault plane into smaller subfaults and treating each these subfaults as a point source. Finally, the response of each subfault is summed up in the time domain to obtain the final time history. The idea of discretization of large events and superimposing the contribution of every small element in the discretized space was first introduced in the original work of Hartzell (1978).

In the finite-fault model, the modeling starts with defining rupture length and width followed with the definition of the subfault dimensions. Each subfault is modeled as point source with an  $\omega^2$  spectrum. One of the subfaults is selected to contain the hypocenter of the modeled event. Rupture propagates radially from the hypocenter with constant rupture velocity. Other subfaults are triggered when the rupture reaches their center. Thus, when obtaining the fault's complete response, the contribution of all subfaults are summed up kinematically with appropriate time delays (Atkinson et al., 2009). The summation is performed in the time domain as follows:

$$a(t) = \sum_{i=1}^{nl} \sum_{j=1}^{nw} a_{ij}(t - \Delta t_{ij} - T_{ij}) \quad (2.20)$$

where  $a(t)$  is the ground motion acceleration from the entire fault whereas  $a_{ij}$  is the ground motion acceleration obtained from the  $ij^{th}$  subfault. Here,  $nl$  and  $nw$  are the number of subfaults along the length and width of main fault, respectively.  $T_{ij}$  is a fraction of rise time of a subfault where the rise time is defined as the subfault radius divided by the rupture velocity (Atkinson et al., 2009). The time delay for each element  $\Delta t_{ij}$ , is the summation of the time required for the rupture front to reach the

element and the time required for the shear-wave to reach the receiver after the element has been triggered (Beresnev and Atkinson 1997). Figure 2.2 displays the fault model, rupture initiation and the wave front on the fault plane.

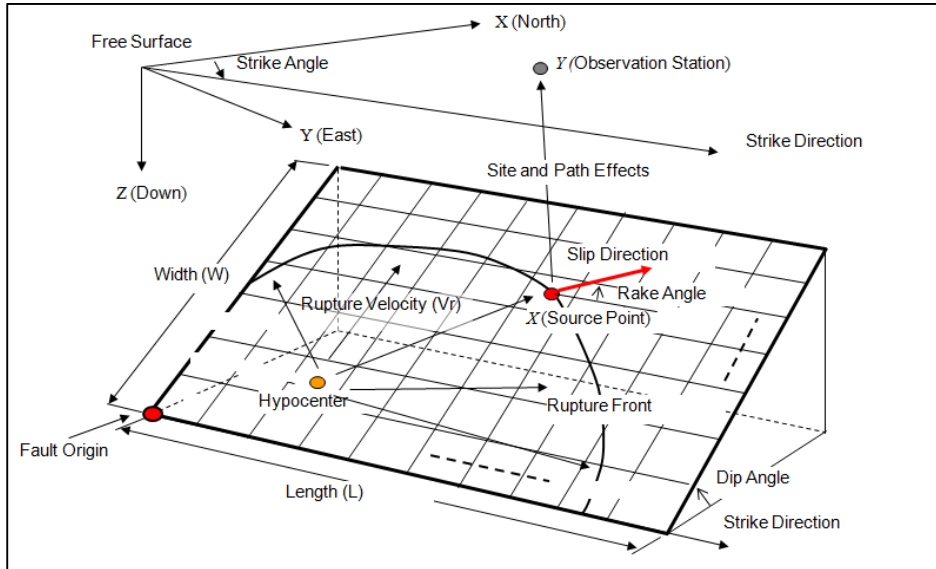


Figure 2.2 Wave propagation on a rectangular finite-fault model (Adapted from Hisada, 2008)

Seismic moment  $M_0$  of each subfault  $ij$ , for  $N$  number of subfaults can be represented as:

$$M_{0ij} = \frac{M_0}{N} \quad (2.21)$$

Equation 2.21 holds as long as the slip rate is assumed to be homogeneous along the fault. If the subfaults are not identical, moment is distributed according to the slip weights of the subfaults (Motazedian and Moinfar, 2006). Then the expression becomes:

$$M_{0ij} = \frac{M_0 S_{ij}}{\sum_{k=1}^{nl} \sum_{l=1}^{nw} S_{kl}} \quad (2.22)$$

where  $S_{ij}$  is the relative slip weight of the  $ij^{\text{th}}$  subfault.

In their early work, Beresnev and Atkinson (1997) defined the Fourier acceleration spectrum of a subfault  $ij$ ,  $A_{ij}$  to be exactly the same with that of stochastic point-source:

$$A_{ij}(f) = \frac{CM_{0ij}(2\pi f)^2}{1 + \left(\frac{f}{f_{c_{ij}}}\right)^2} \left(\frac{1}{R_{ij}}\right) e^{-\frac{\pi f R_{ij}}{Q\beta}} D(f) e^{-\pi\kappa f} \quad (2.23)$$

where the (static) corner frequency of a subfault,  $f_{c_{ij}}$  is defined as:

$$f_{c_{ij}} = 4.9 * 10^6 \beta \left(\frac{\Delta\sigma}{M_{0ij}}\right)^{\frac{1}{3}} \quad (2.24)$$

The original program utilizing the stochastic finite-fault method, FINSIM (Beresnev and Atkinson, 1998), used this static corner frequency approach. However, in this approach the simulated acceleration spectrum was dependent on the subfault size and number of subfaults. Motazedian and Atkinson (2005) addressed this issue by introducing the dynamic corner frequency approach. In dynamic corner frequency approach, while the rupture propagates the corner frequency changes inversely proportional to ruptured area at that time. The dynamic corner frequency is expressed as follows:

$$f_{cij} = N_R(t)^{-\frac{1}{3}} 4.9 * 10^6 \beta \left( \frac{\Delta\sigma}{M_{0ave}} \right)^{\frac{1}{3}} \quad (2.25)$$

where  $N_R(t)$  is the cumulative number of ruptured subfaults at time  $t$ ,  $M_{0ave} = M_0/N$  is the average seismic moment of subfaults.

As rupture progresses, number of ruptured subfaults increase and the corner frequency decreases thus the radiated energy in the high frequencies. In order to conserve radiated energy at higher frequencies, Motazedian and Atkinson (2005) applied a frequency-dependent scaling factor  $H_{ij}$  to the spectrum. With this modification, acceleration spectrum finally becomes:

$$A_{ij}(f) = \frac{CM_{0ij}H_{ij}(2\pi f)^2}{1 + \left(\frac{f}{f_{cij}}\right)^2} \left(\frac{1}{R_{ij}}\right) e^{-\frac{\pi f R_{ij}}{Q(f)\beta}} D(f) e^{-\pi\kappa f} \quad (2.26)$$

$$\text{where } H_{ij} = \left( N \frac{\sum \frac{f^2}{1 + \left(\frac{f}{f_c}\right)^2}}{\sum \frac{f^2}{1 + \left(\frac{f}{f_{cij}}\right)^2}} \right)^{\frac{1}{2}}$$

Lastly, Motazedian and Atkinson (2005) introduced another modification to the stochastic finite-fault methodology. The pulsing percent is defined as the ratio of maximum rupture area to the entire fault area. Until pulsing percent is reached, the rupture propagates and dynamic corner frequency decreases.

Finally, in this thesis, the stochastic finite-fault model is employed in the same fashion as developed in Motazedian and Atkinson (2005) and described in this Chapter.



## **CHAPTER 3**

### **GROUND MOTION SIMULATIONS IN BURSA REGION**

#### **3.1 General**

In this chapter, stochastic finite-fault simulations of real ground motions recorded in Bursa region are performed. The objective of these simulations is to calibrate the regional model parameters and obtain a reliable model for the scenario earthquake simulations. For this purpose, regional seismic parameters are investigated and the optimum parameters are obtained by verification of the synthetic records with the real ones. The attenuation of the simulated records are also compared against existing ground motion prediction equations.

In section 3.2, background information about seismicity and tectonics of Bursa region is presented. In section 3.3, selected strong ground motions are investigated. In section 3.4, estimation of optimum model parameters are discussed. Results of the simulations in terms of comparisons with real records and ground motion prediction equations are presented in section 3.5.

#### **3.2 Background information**

Bursa region is located in the south of Middle Strand of North Anatolian Fault Zone (MS-NAF) and north of the Southern Strand of North Anatolian Fault Zone (SS-NAF) and the Inonu-Eskisehir Fault Zone (IEFZ). SS-NAF extends to Ulubat fault

(UF) which is located south of Ulubat Lake (Yaltirak, 2002) and west of the study region. In addition, there are several seismically active normal and strike-slip faults and fault segments in the region such as the Gemlik Fault (GF), Geyve-Iznik Fault Zone (GIFZ), Yenisehir Fault (YNF), and the Bursa Fault (BF) (Gok and Polat, 2011). Figure 3.1 shows the major faults near Bursa region. One of the most damaging historical earthquakes in this area happened on 28 February 1855, with an intensity value of  $I_0 = X$  ( $M_S = 7.1$ ) (Ambraseys, 2000; 2002)

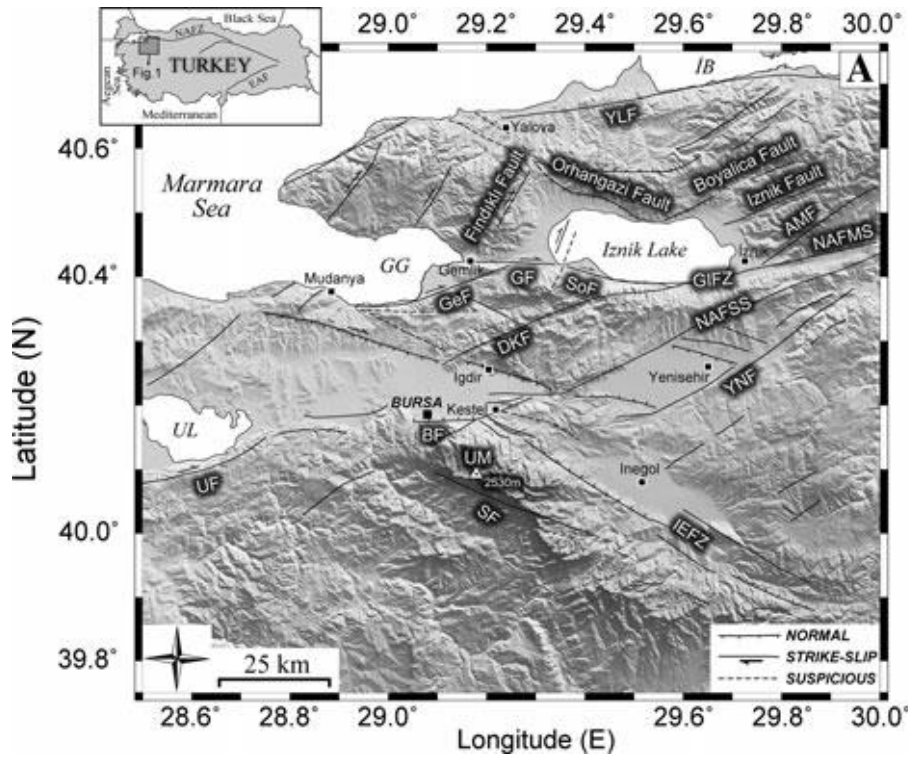


Figure 3.1 Major faults near Bursa Region. (AMF: Adliye Mesruriye Fault, BF: Bursa Fault, DKF: Demirtas-Kiblepinar Fault, GeF: Gencali Fault, GF: Gemlik Fault, GG: Gemlik Gulf, GIFZ: Geyve-Iznik Fault Zone, IEFZ: Inonu-Eskisehir Fault Zone, NAFMS: North Anatolian Fault Middle Strand, NAFSS: North Anatolian Fault Southern Strand, SF: Sogukpinar Fault, SoF: Soloz Fault, UF: Uluabat Fault, UL: Uluabat Lake, UM: Uludağ Mountain, YLF: Yalova Fault, YNF: Yenisehir Fault (Adapted from Gok and Polat, 2011)

### 3.3 Strong Ground Motion Dataset

As strong ground motions used in this study, ground motions within 200 km distance of Bursa city center with  $M_W \geq 4.5$  are selected. A total of 4 earthquakes are selected according to these criteria. In Table 3.1 information of the selected earthquakes are presented.

Table 3.1 Selected earthquakes near Bursa City

Epicenter Location	Epicenter Latitude (°N)	Epicenter Longitude (°E)	Earthquake Date	M <sub>w</sub>
Bilecik	40.14	29.96	2011.07.11	4.9
Karacabey	40.27	28.32	2006.12.19	4.9
Keles	39.88	29.28	2003.12.23	4.8
M.Kemalpasa	39.99	28.67	2003.03.20	4.6

Location of the epicenters of the selected earthquakes and the stations that recorded these events are displayed in Figure 3.2.

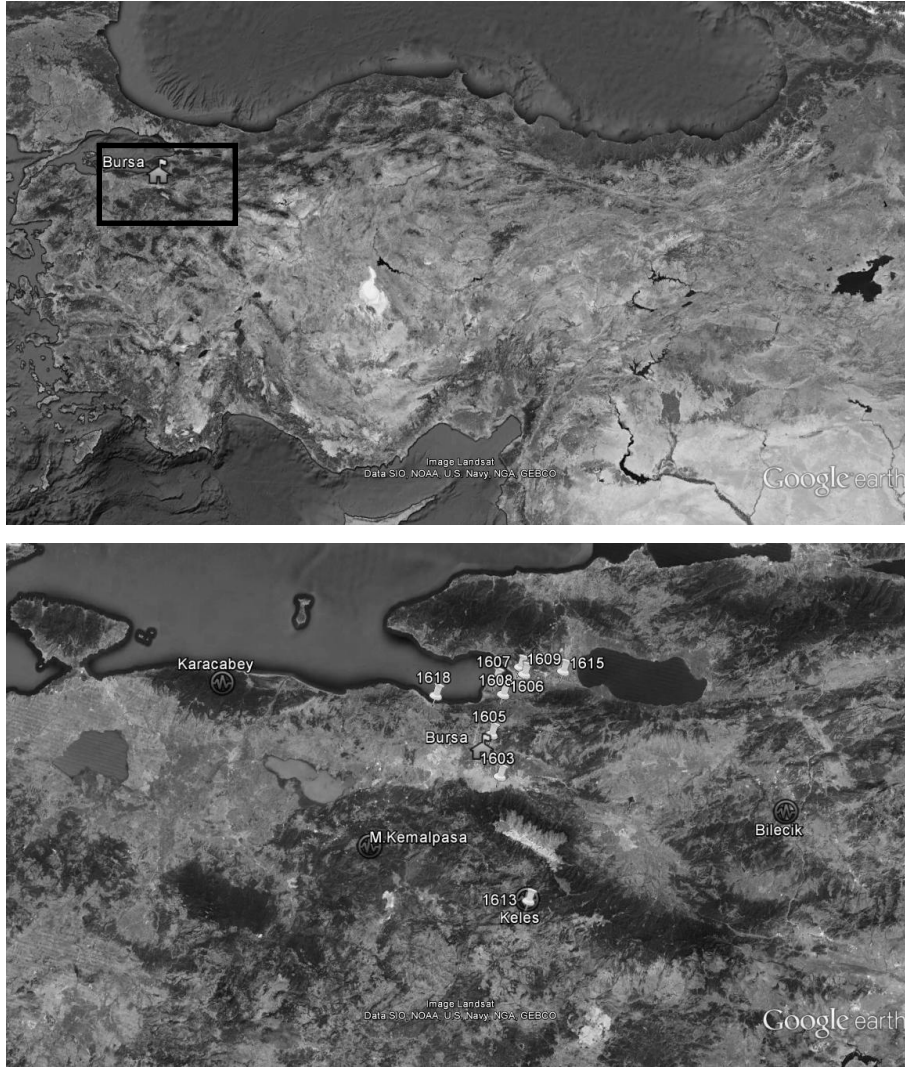


Figure 3.2 Location of the epicenters of the selected earthquakes and the recording stations

The raw versions of the corresponding ground motion records are obtained from DAPHNE database ([http://kyhdata.deprem.gov.tr/2K/kyhdata\\_v4.php](http://kyhdata.deprem.gov.tr/2K/kyhdata_v4.php)). Baseline correction and forth-order Butterworth filter with a band-pass frequency range of 0.25-25Hz is applied to the raw ground motion records. Information on the stations that recorded these earthquakes is given in Tables 3.2-3.5. A total of 33 stations in the study area is considered in this thesis.

Table 3.2 Information on stations that recorded Bilecik earthquake

Station Code	Latitude (°N)	Longitude (°E)	$V_{s30}$ (m/s)	$R_{jb}$ (km)	PGA (cm/s <sup>2</sup> )	
					(NS)	(EW)
1613	39.915	29.232	401	66.90	5.96	5.02
1618	40.351	28.928	310*	91.01	15.17	16.61

\*: There is no information about the  $V_s$  profile at station 1618. In ground motion simulations, this site is modeled as generic soil with  $V_{s30} = 310$  m/s as suggested by Boore and Joyner (1997).

Table 3.3 Information on stations that recorded Karacabey earthquake

Station Code	Latitude (°N)	Longitude (°E)	$V_{s30}$ (m/s)	$R_{jb}$ (km)	PGA (cm/s <sup>2</sup> )	
					(NS)	(EW)
1603	40.182	29.127	459	71.05	1.50	1.49
1605	40.273	29.096	488	66.37	2.06	3.70
1606	40.363	29.122	274	68.18	3.74	4.61
1607	40.394	29.098	370	66.35	2.77	2.18
1608	40.410	29.179	366	73.39	2.40	2.82
1609	40.425	29.167	228	72.51	3.54	4.00
1613	39.915	29.232	401	90.89	3.64	3.62

Table 3.4 Information on stations that recorded Keles earthquake

Station Code	Latitude (°N)	Longitude (°E)	$V_{s30}$ (m/s)	$R_{jb}$ (km)	PGA (cm/s <sup>2</sup> )	
					(NS)	(EW)
1606	40.363	29.122	274	49.62	3.44	3.43
1615	40.422	29.291	348	55.72	2.11	3.27

Table 3.5 Information on stations that recorded M.Kemalpasa earthquake

Station Code	Latitude (°N)	Longitude (°E)	$V_{s30}$ (m/s)	$R_{jb}$ (km)	PGA (cm/s <sup>2</sup> )	
					(NS)	(EW)
1605	40.273	29.096	488	40.23	6.16	3.69
1606	40.363	29.122	274	49.34	7.97	11.61
1607	40.394	29.098	370	51.07	2.14	2.31
1608	40.410	29.179	366	56.48	1.57	1.76
1615	40.422	29.291	348	63.61	2.20	1.97

### 3.4 Model Parameters

In order to obtain accurate ground motion estimations; source, path and site properties must be properly represented in the stochastic finite-fault model. Deriving these input parameters from regional data yields the most reliable outcome, however

generic values should be utilized when the regional data do not exist or are insufficient (Askan et al., 2013).

### 3.4.1 Source parameters

Source properties are defined in the stochastic finite-fault simulations with the following input parameters: Coordinates and depth of the upper edge of the fault, dip and strike angles, rupture length and width, hypocentral depth and coordinates, slip distribution along the fault plane, stress drop, and pulsing area percentage. In this thesis, dip and strike angles, hypocentral depth and coordinates are obtained from the focal solutions of the earthquakes. Fault coordinates are obtained from active fault map of Turkey. Rupture length and width are estimated by using empirical equations of Wells and Coppersmith (1994). Random slip distributions, which are compatible with the moment magnitude of the events, is used herein.

Pulsing area percentage parameter controls the low frequency portion of the Fourier Amplitude Spectrum. This parameter is generally obtained by constraining other parameters and minimizing the errors between synthetic and observed ground motions with an iterative process (Motazedian and Atkinson, 2005). Since this parameter is different for each earthquake, calibrating the model with this parameter might yield unreliable results in the scenario earthquake simulations. Therefore, this parameter is fixed at 50%.

Stress drop is the stress difference between the start and the end of the rupture process. Estimation of this parameter involves inherent uncertainties, thus it can not be easily determined. For the reliability of the scenario earthquake simulations, this parameter is also not included at the parameter optimization. An empirical relationship proposed by Mohammadioun and Serva (2001) is used for the estimation of stress drop. The relationship is as follows:

$$\sigma_{SS} = 8.9 \times W^{0.8} \quad (3.1)$$

where  $\sigma_{SS}$  is the stress drop and  $W$  is the width of the rupture surface.

### 3.4.2 Path parameters

Geometric spreading, distance-dependent duration and frequency-dependent anelastic attenuation (quality factor) define the path model. In Bursa region, the geometric spreading model proposed by Ansal et al. (2009) for Marmara Region is used.

$$\begin{aligned}
 R^{-1} & R \leq 30 \text{ km} \\
 R^{-0.4} & 30 \text{ km} < R \leq 60 \text{ km} \\
 R^{-0.6} & 60 \text{ km} < R \leq 90 \text{ km} \\
 R^{-0.8} & 90 \text{ km} < R \leq 100 \text{ km} \\
 R^{-0.5} & R > 100 \text{ km}
 \end{aligned} \tag{3.2}$$

As there is no regional model, distance-dependent duration model is adapted from Herrmann (1985). This model is employed effectively in many past studies (e.g.: Ugruhan and Askan, 2010; Askan et al., 2013). The model equation is given as:

$$T = T_0 + 0.05R_{hypo} \tag{3.3}$$

where  $T_0$  is the source duration in seconds,  $R_{hypo}$  is the hypocentral distance in km.

Two models exist for the Bursa region's anelastic attenuation: The models by Horasan et al. (1998) and by Akyol et al. (2002) are tested as the quality factor in this study. In addition, a generic model proposed by Boore (1984) which utilize the world-wide ground motion data is considered.

### 3.4.3 Site parameters

Site effects are defined with site amplification and  $\kappa_0$  (site diminution) parameters. As mentioned in the Chapter 2, site parameters have significant impact on the amplitude of the target spectrum. Therefore, selection of these parameters is extremely important for an accurate ground motion output.

In order to reflect the amplification effects at the sites accurately, three alternative approaches are tested. Four stations (1610, 1611, 1612 and 1614) had borehole logs provided at the online DAPHNE database. Vs30 values for all stations were also provided there. Since 1-D theoretical site response analysis requires soil layer information, tests are conducted at these four stations. Borehole depths for these stations are between 12.50 meters and 40.77 meters. (Borehole information at the stations is only available down to a maximum of 40.77 meters). Thus, there is no information about the bedrock depth and the soil profile between bedrock and end of the borehole. As a result, using the soil layer data and SPT counts, geotechnical properties of the sites are estimated. For sands closer to surface, Seed and Idriss (1991) Lower Bound reference curve is used to account for the damping of looser soils. Similarly, for sand layers deeper into the soil profile Seed and Idriss (1991) Upper bound is used since much lower damping values are expected from stiffer layers. In addition, extra layers are modeled under the borehole depth in order to prevent drastic changes in the shear wave velocities between bedrock and the site. In this empirical application, shear wave velocity of the extra layers are assumed to be linearly decreasing 100 m/s for every 10 meters down to the bedrock. Equivalent linear approach in DeepSoil Software is used for the 1-D theoretical site response analysis. Sakarya record from the 17 August 1999 Kocaeli event is used as input motion in this study. Since Sakarya station is on very dense soil/soft rock conditions (with NEHRP site class C), this record is employed as input at the bedrock layer for all stations. The resulting transfer function at the surface layer is the amplification function for the site.

Amplification factors are also calculated using the empirical H/V approach described in Chapter 2. Following this method, Horizontal Fourier Amplitude

Spectrum to Vertical Fourier Amplitude Spectrum ratio of the S-wave portion of each available record is computed for all stations. Then, at every station, the absolute mean of these H/V values yield the empirical amplification spectrum of that site. In order to compare H/V with other amplifications, another adjustment must be made: Although in H/V method vertical component of the record is assumed to be free from the effects of the site conditions, near-site attenuation still applies. Therefore, H/V term also includes  $\kappa_{0_{Horizontal}}/\kappa_{0_{vertical}}$  term. Thus, to make all amplification methods comparable and consistent with each other, vertical kappa factor should be employed in the simulations when using H/V method (Motazedian, 2006).

The third alternative for site amplification factors is the generic amplification spectra by Boore and Joyner (1997). In this method, Boore and Joyner (1997) proposed amplification functions for NEHRP class C ( $\bar{V}_{30}=520\text{m/s}$ ), NEHRP class D ( $\bar{V}_{30}=255\text{m/s}$ ) and generic soil ( $\bar{V}_{30}=310\text{m/s}$ ) sites. Proposed functions assumes  $\kappa_0 = 0.035$  calculated from empirical studies at western North America. Amplification functions provide 11 frequency-amplification data points. In this study, local  $\kappa_0$  values are calculated for each station as presented in the next section. The amplification values between 0.5Hz and 10Hz (Boore and Joyner, 1997) are adjusted with local  $\kappa_0$  values using the adjustment factor  $\exp[-\pi(\kappa_0 - \kappa_{new})f]$  for frequency  $f$  suggested by Boore and Joyner (1997). In this adjustment factor  $\kappa_0$  corresponds to the western North American  $\kappa_0 = 0.035$ , and  $\kappa_{new}$  is the local  $\kappa_0$  calculated in this study.

Site amplifications from these alternative techniques are compared with each other in Figures 3.3-3.9. H/V amplification at a site is calculated as  $H/V \times e^{(-\pi \times f \times \kappa_{0_{vertical}})}$  at every frequency  $f$ . Site amplification is calculated from Boore and Joyner (1997) generic amplification spectra ( $BJ$ ) as  $BJ \times e^{(-\pi \times f \times \kappa_{0_{horizontal}})}$  for every frequency  $f$ . Theoretical transfer functions (TTF) are calculated at stations 1610, 1611, 1612 and 1614 with DeepSoil software. The modified Vs profiles of these stations are also displayed in Figures 3.4, 3.5, 3.6 and 3.8.

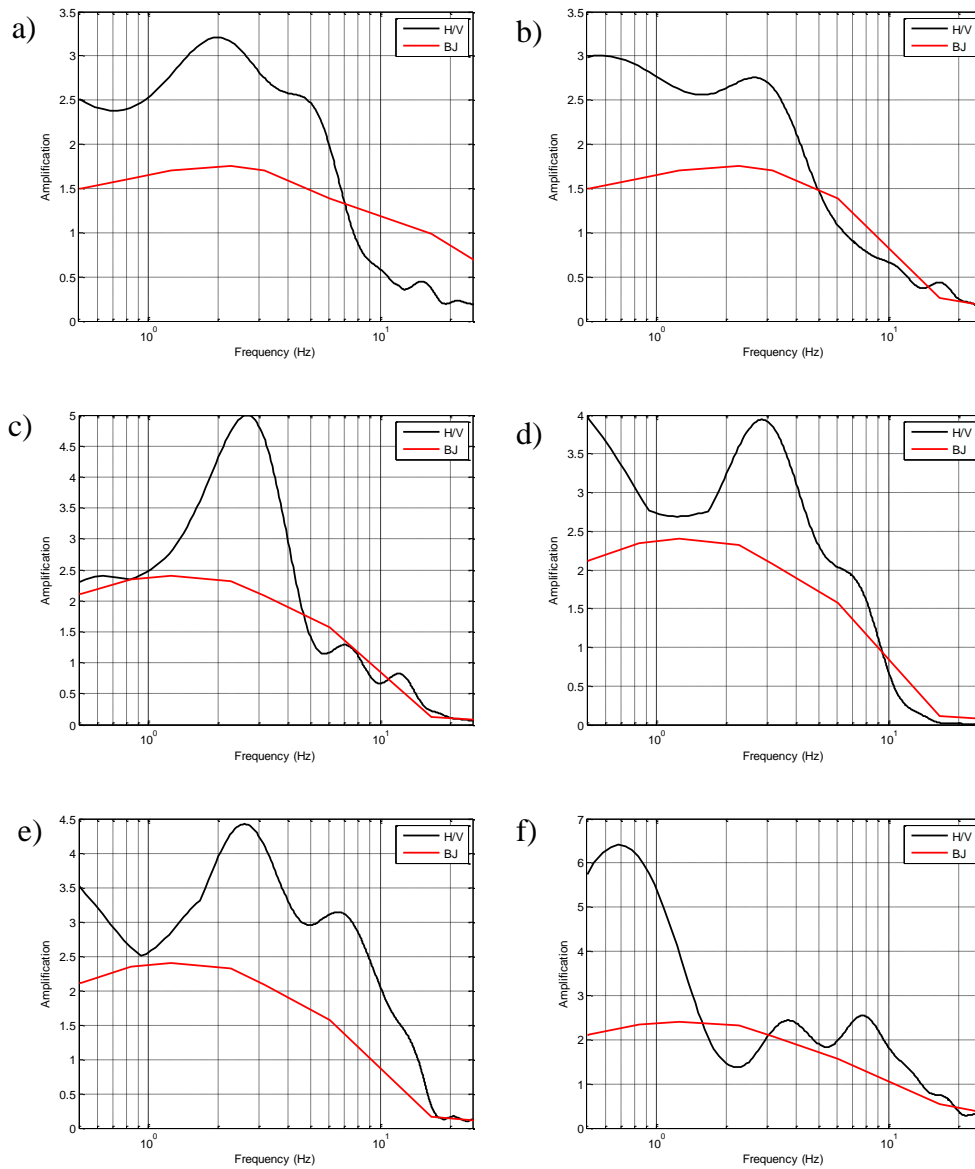


Figure 3.3 Site amplification from alternative techniques at station a)1603, b)1605, c)1606, d)1607, e)1608 and f)1609

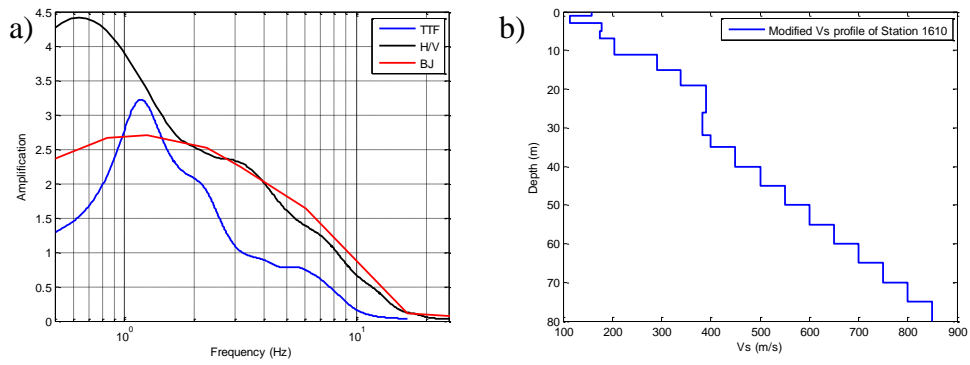


Figure 3.4 Site amplification from alternative techniques at station 1610 b) Modified Vs profile of Station 1610

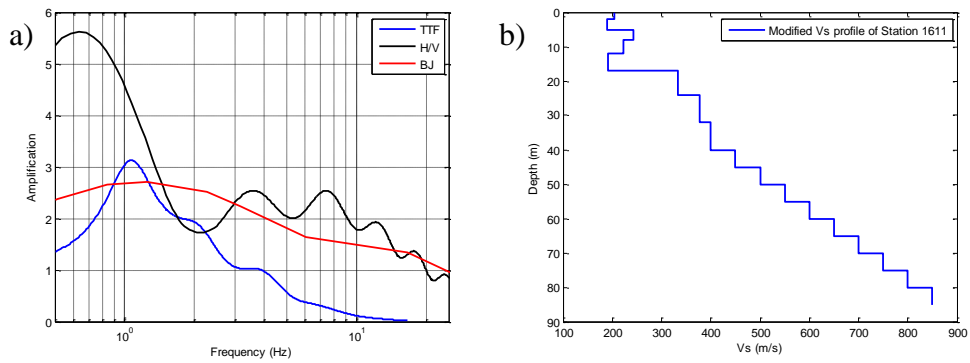


Figure 3.5 Site amplification from alternative techniques at station 1611 b) Modified Vs profile of Station 1611

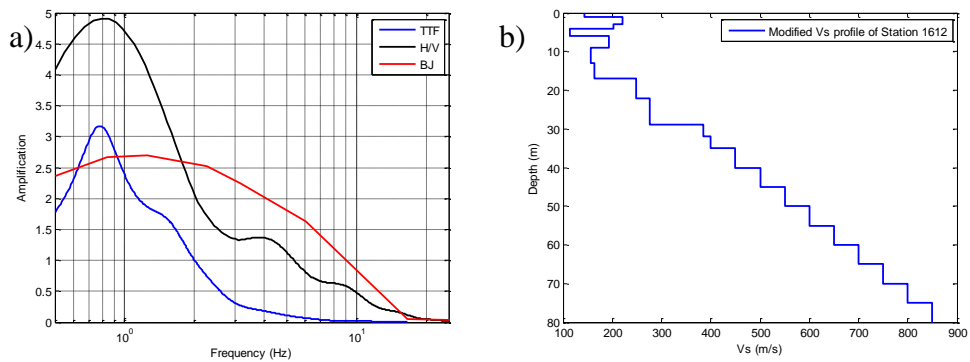


Figure 3.6 Site amplification from alternative techniques at station 1612 b) Modified Vs profile of Station 1612

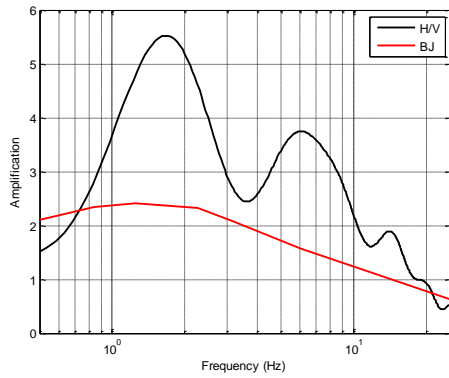


Figure 3.7 Site amplification from alternative techniques at station 1613

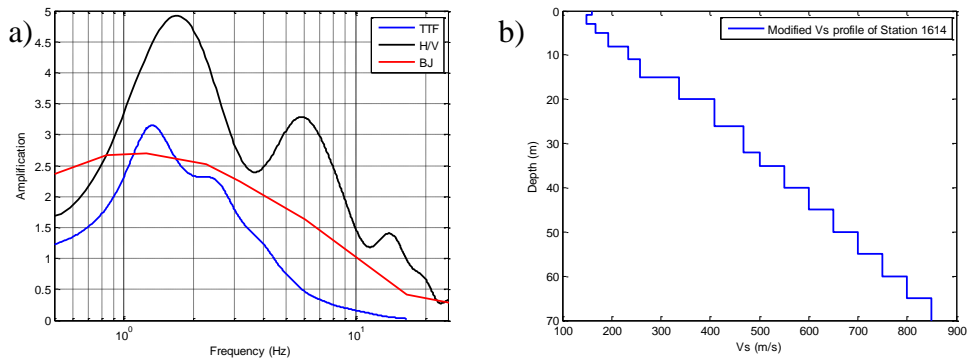


Figure 3.8 Site amplification from alternative techniques at station 1614 b) Modified Vs profile of Station 1614

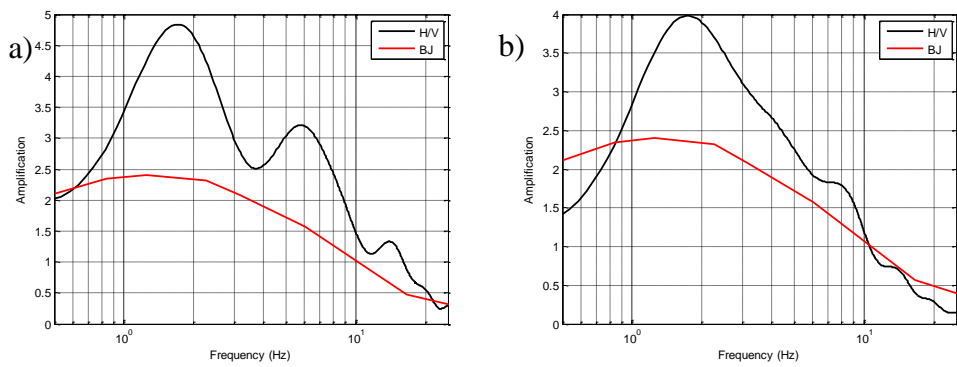


Figure 3.9 Site amplification from alternative techniques at station a) 1615 and b) 1618

Figures 3.3–3.9 reveal that the fundamental peak from the TTF match the first peak of the H/V spectra at most of the stations. However, H/V spectra typically display more peaks than TTF. This could point to the multi-mode seismic energy present in the earthquake records or the mean H/V spectra revealing pseudo peaks. On the other hand, when BJ spectra is compared to the others, there is no clear peak at the fundamental frequency as in the H/V spectra or the TTF. Yet, despite its generic form, the BJ spectra is observed to follow the general trend of the TTF except for the very high frequencies. When the amplitudes are considered, it is observed that the H/V spectra yields an overestimation at all frequencies while the TTF and BJ spectra yield close matches with each other around the fundamental frequency. Indeed, it is discussed in several previous studies (Bonilla et al., 2002; Field and Jacob, 1995; Panzera et al., 2011) that despite efficiency of H/V method in estimating the fundamental frequency of soils, the corresponding amplitudes are not accurate. This is mostly probably due to the fact that the source effects that cannot be totally eliminated in H/V method.

Finally, TTF cannot be computed at all stations of interest due to lack of 1D soil profiles. Thus, in the light of the previous discussions, a comparison between BJ spectra and H/V method leads to the use of BJ model since it yields considerably similar results with TTF. In the simulations, BJ models corresponding to the soil types at the stations is employed. The highest amplification with BJ model is observed at station 1610. This is expected since the  $V_{s30}$  of this site is one of the lowest in the region. It is also observed that stations in the northern Bursa generally have higher site amplifications than the stations in southern Bursa.

The other site parameter is the diminution factor kappa zero. Kappa values are determined by the method developed by Anderson and Hough (1984). As the first step S-wave portion of the records are selected. Then Fourier amplitude acceleration spectrum are plotted. In semi-logarithmic plots, limiting frequencies of  $f_0$  and  $f_{max}$  are selected manually. The frequency  $f_0$  is the beginning of the exponential decay and the  $f_{max}$  is the maximum frequency where exponential decay can be distinguished from the noise. Finally, linear regression is performed between  $f_0$  and  $f_{max}$ . The slope of the best fit line is  $-\pi\kappa$ . From here  $\kappa = -Slope/\pi$  is calculated for

an individual component of a ground motion record. In order to decrease the effect of error caused by this manual selection method, kappa analyses are performed 4 times, and each 3 component of the records are processed individually in this thesis. Thus for a single record, 8 data points for horizontal and 4 data points for vertical kappa is obtained. Median of the 8 horizontal and median of the 4 vertical kappa values are used in order to eliminate bias caused by potential outliers and any subjective errors. Moreover, data that are recorded outside of 350km epicentral distance range are rejected to eliminate path effects. This function is obtained by a linear best fit to the kappa vs. epicentral distance trends. The value at epicentral distance=0km is defined as Kappa zero. It is the kappa of the site without the path effects and this value is used in the stochastic ground motion simulation procedure. Kappa models for the stations are presented in Figures 3.10-3.12

In this study, it is observed that as the soil gets softer,  $\kappa_0$  increases. This is theoretically expected due to higher near-surface attenuation in softer soil media leading to steeper decay of higher frequencies. Yet, at some stations, most probably due to limited number of data points in the kappa models, such a correlation could not be observed. Even though kappa calculation process was repeated 4 times, dispersions are observed at some stations. These dispersions are believed to arise not from the kappa calculations but from the low data quality. These data-related issues in this study points out to the need for high-quality and complete seismic datasets in Turkey.

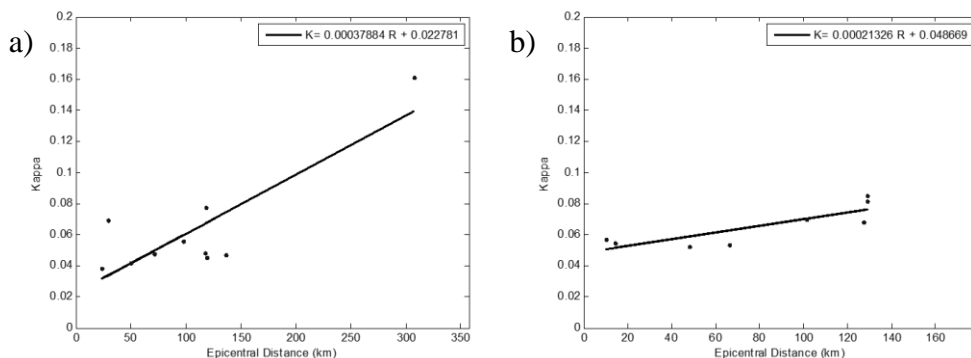


Figure 3.10 Horizontal kappa model of station a)1603 and b)1605

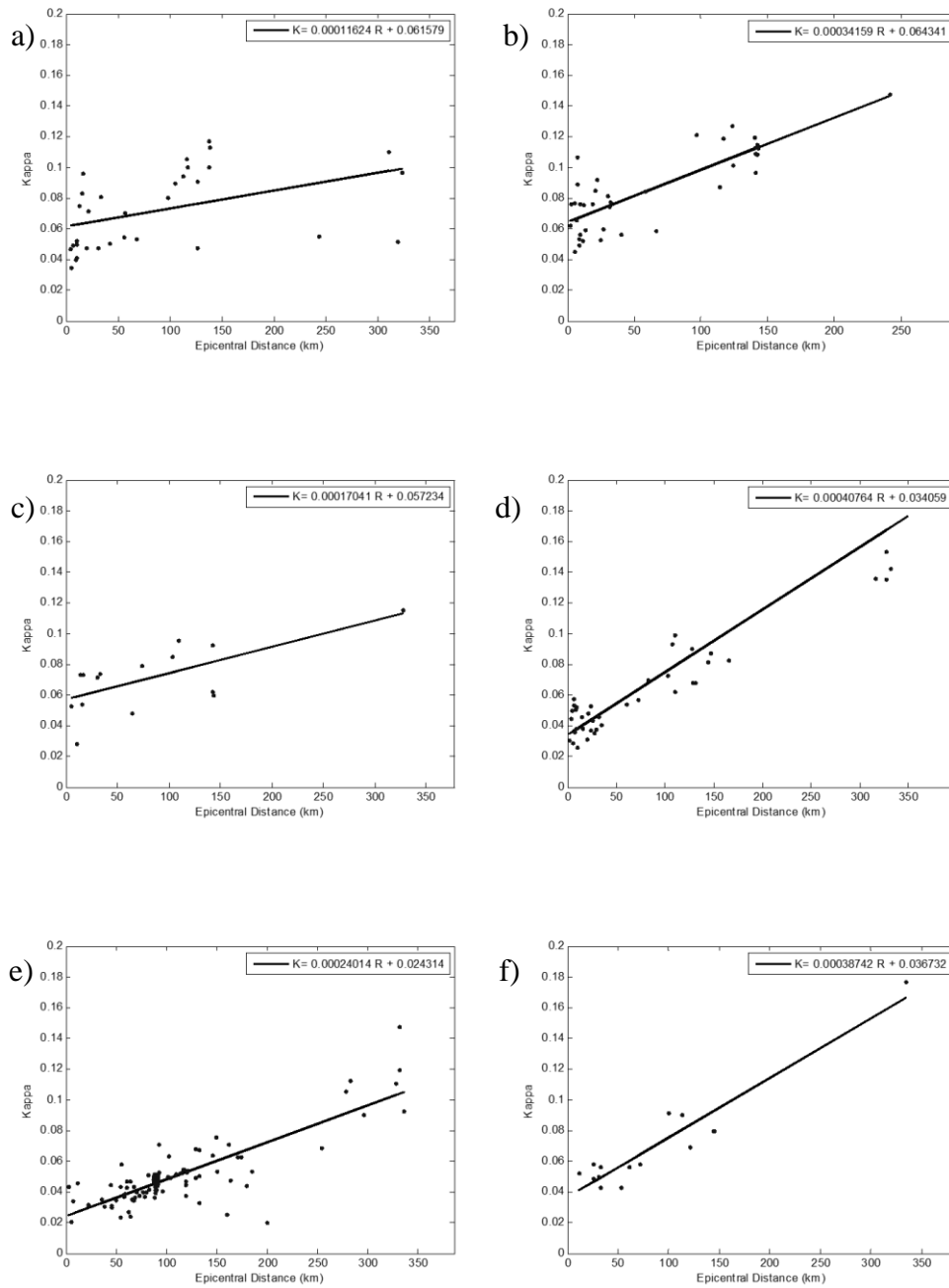


Figure 3.11 Horizontal kappa model of station a)1606, b)1607, c)1608, d)1609, e)1613 and f)1615

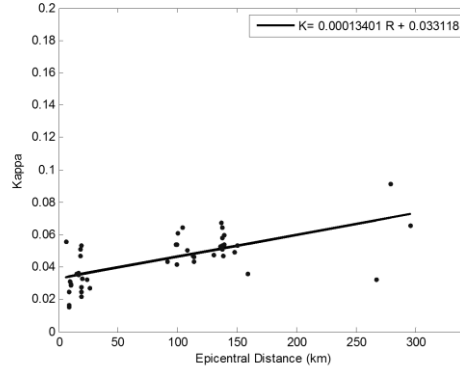


Figure 3.12 Horizontal kappa model of station 1618

### 3.5 Optimization for Model Parameters

There are several options for selecting path and site parameters due to the uncertainties involved in the modeling process. In this thesis, an error minimization scheme is utilized to choose the optimum values of the parameters. Error (misfit) function is defined as follows:

$$E(f) = \log \left( \frac{A(f)_{observed\ ave}}{A(f)_{synthetic}} \right) \quad (3.5)$$

where  $A(f)$  is the amplitude of the Fourier acceleration spectra at frequency  $f$ . Here average observed record,  $A(f)_{observed\ ave}$ , is defined as square root of multiplication of the NS and EW components. This error minimization process is utilized for each recording for frequencies between 0.5Hz-25Hz. Three variables are considered herein; quality factor, amplification factor and kappa. There are two main constraints for parameter search; the quality factor of a region must be the same for each earthquake and the site effects must be the same at a site for every event. Three different quality factor formulations are selected from the literature. These models are shown in Figure 3.13.

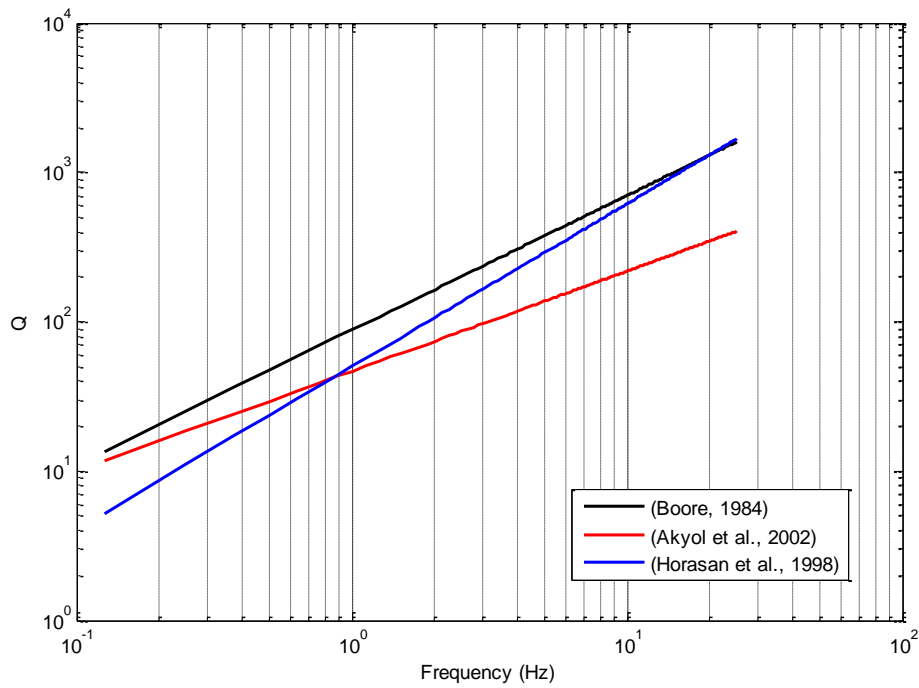


Figure 3.13 Quality factor options for parameter optimization

After the initial error minimization process, it is observed that for the Bursa region, the optimum quality factor model is found to be  $Q_s = 50f^{1.09}$ , by Horasan et al. (1998). As the amplification factor, the generic rock amplification proposed by Boore and Joyner (1997) is utilized.

After other parameters are fixed, kappa parameter is tested. Since kappa estimation process is manual and might involve subjective bias, 3 options are considered; lowest  $\kappa_0$  of the region (0.0228, obtained from station 1603), highest  $\kappa_0$  of the region (0.0643, obtained from station 1607) and the  $\kappa_0$  of the station under consideration. For most cases  $\kappa_0$  of the station under considerations yields the lowest error. However, for stations 1603 and 1615 using the highest  $\kappa_0$  of the region resulted in smaller misfits. Optimum parameter sets used in the verification simulations are shown in the Table 3.6.

Table 3.6 Parameters used for verification simulations

Epicenter location	Bilecik	Karacabey	Keles	M.Kemalpasa
Date	2011	2006	2003	2003
Mw	4.9	4.9	4.8	4.6
Hypocenter Latitude (N)	40.14	40.27	39.88	39.99
Hypocenter Longitude (E)	29.96	28.32	29.28	28.67
Depth from surface (km)	23.1	16.75	13.3	4.35
Strike	45	45	45	135
Dip	90	90	90	90
Fault dimensions	3×3.5	3×3.5	2.5×3	2×2.5
Subfault dimensions	0.5×0.5	0.5×0.5	0.5×0.5	0.5×0.5
Crustal shear wave velocity(km/s)	3.5			
Crustal density (g/cm <sup>3</sup> )	2.8			
Rupture velocity(km/s)	2.8			
Stress drop (bar)	24	24	21	18.5
Pulsing Area percent	50			
Quality factor	$50f^{1.09}$			
Geometric spreading	$R^{-1}, R \leq 30 \text{ km}$ $R^{-0.6}, 30 \text{ km} < R \leq 100 \text{ km}$ $R^{-0.5}, 100 \text{ km} < R$			
Duration model	$T = T_0 + 0.05R$			
Windowing function	(Saragoni and Hart 1973)			
Kappa factor	Site specific $\kappa_0$ (0.0643 for stations 1603 and 1615)			
Site amplification factor	(Boore and Joyner, 1997)			

### 3.6 Simulation Results

#### 3.6.1 Comparison of Simulated and Observed Data

Using the optimized parameters, 4 earthquakes are simulated. For 9 stations, a total of 14 simulated records are obtained. These synthetic records are compared with their corresponding observations. Records are compared according to their frequency content, amplitude and duration. Comparisons are made in terms of Fourier Amplitude Spectrums and acceleration time histories. Simulation results along with the error between synthetic and observed records are presented in Figures 3.14-3.17. In these figures, red and blue lines are the two horizontal (East-West and North-South) components of the observed records and the black lines are the synthetic records. In the error versus frequency plots, the average error values are presented. Finally, the error in Figures 3.28-3.31 is as defined in Equation 3.5.

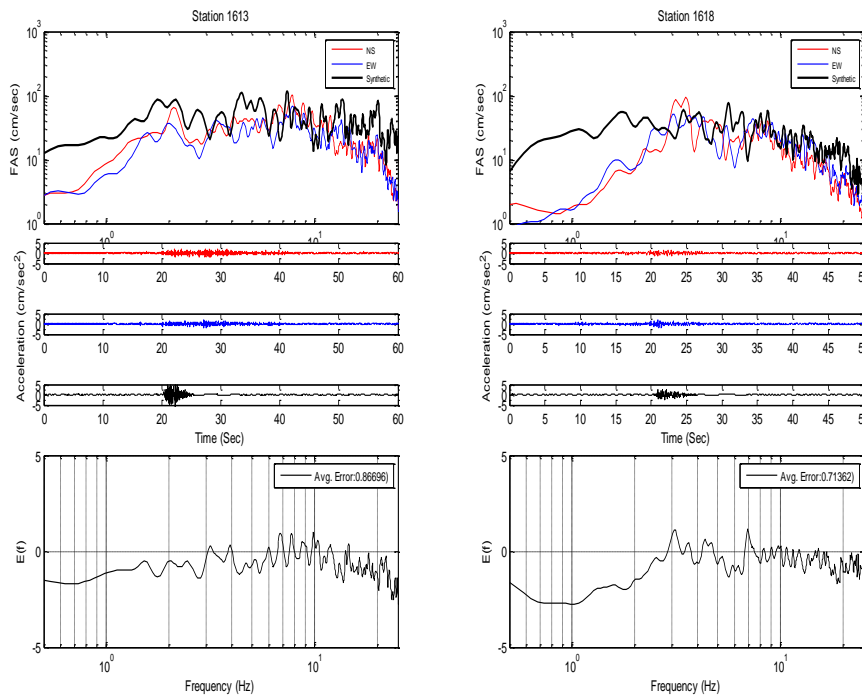


Figure 3.14 Comparison of Observed and Simulated Records for Bilecik Earthquake

Bursa simulation model parameters defined Bilecik earthquake well. Except for the frequencies less than 1 Hz (that cannot be effectively simulated with the stochastic

method), the synthetic records are in close match with the observed records. The high frequency spectral content at both stations is accurately simulated. Ground motion duration of the synthetic record is shorter at station 1613 most probably due to the lack of surface waves in the simulation method. The amplitudes at the very high frequencies ( $>10$  Hz) of the simulated record at 1613 are slightly overestimated. Duration and amplitude of the synthetic record is similar to the observed record at station 1618. For both stations, error plots show that there is no systematic bias at any particular frequency level.

Simulations for Karacabey earthquake yields accurate results for the frequency range 0.5-25Hz at station 1607. For stations 1603, 1605 and 1609, despite the close match at high frequencies, there is an overestimation of the low frequency spectral amplitudes. The misfit at lower frequencies might be a result of the source effects that could not modeled accurately in the stochastic method. The high frequency content is effectively modeled with the regional path and local site parameters. The high frequency decay is also modeled effectively with the local kappa models at most stations. Finally, S-wave durations are obtained to be very similar to those of the observed records. At station 1606, the estimations are accurate between frequencies 3-9 Hz. There is a slight underestimation at higher frequencies at this station. Similarly at station 1608, the intermediate frequencies are estimated accurately, yet after 10Hz synthetic starts to underestimate.

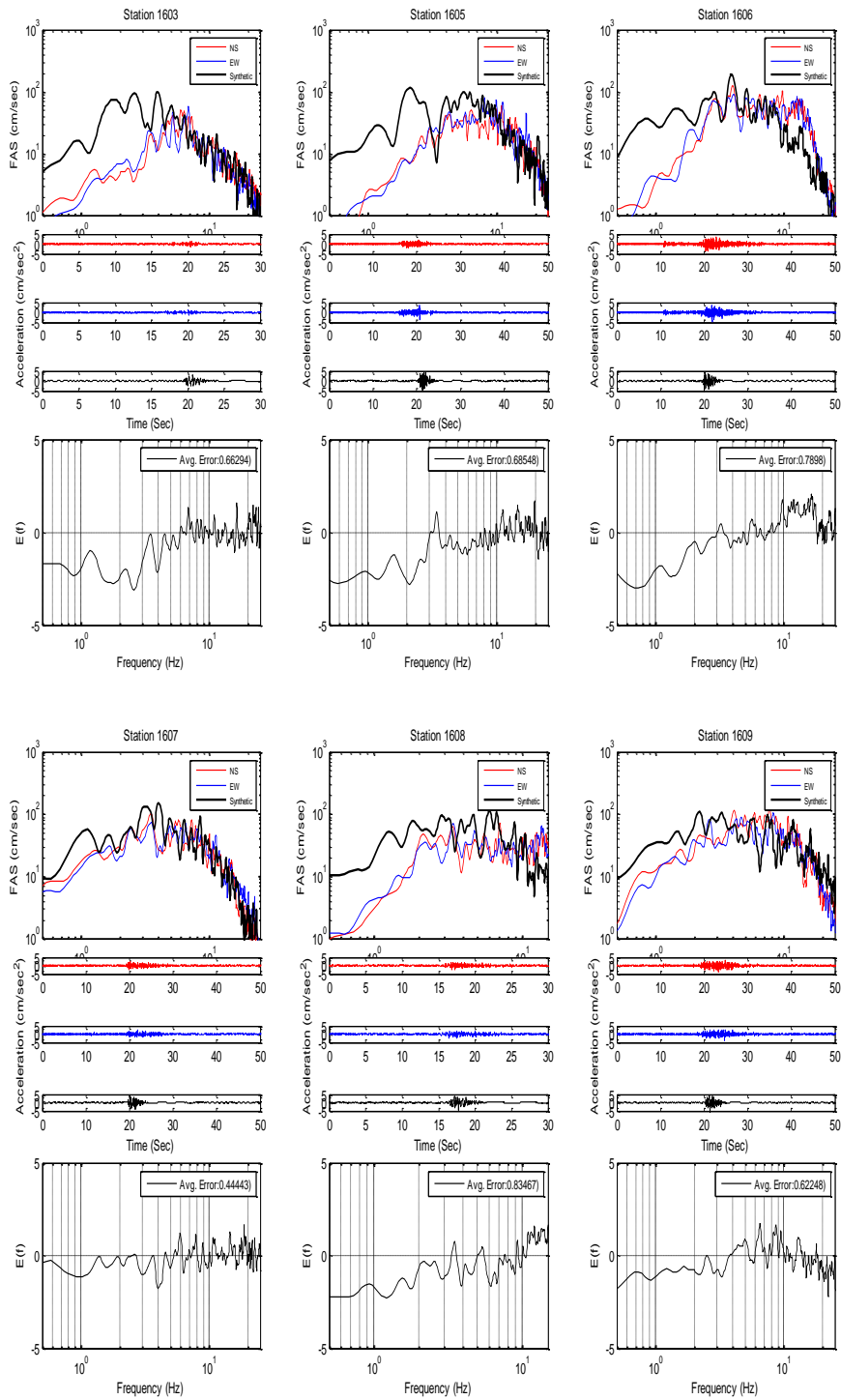


Figure 3.15 Comparison of Observed and Simulated Records for Karacabey Earthquake

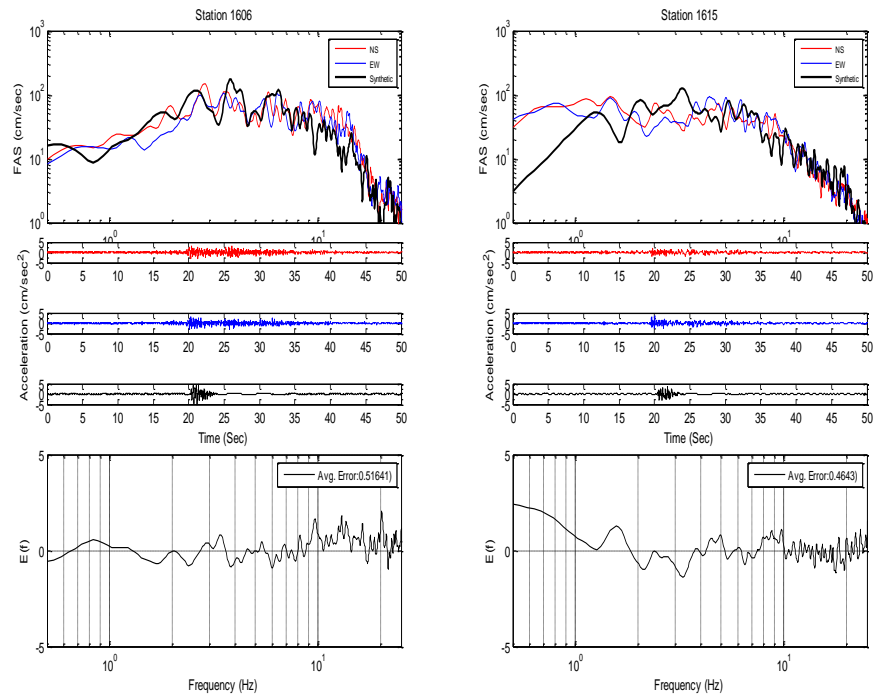


Figure 3.16 Comparison of Observed and Simulated Records for Keles Earthquake

Simulation of Keles event shows that the synthetic spectra at station 1606 is very accurate at all frequencies (including the source-related low frequencies). A similar observation holds at station 1615 where the simulation is accurate between 1Hz and 25Hz. Finally, S-wave durations of the simulated records are similar to those of the observed records at stations 1606 and 1615.

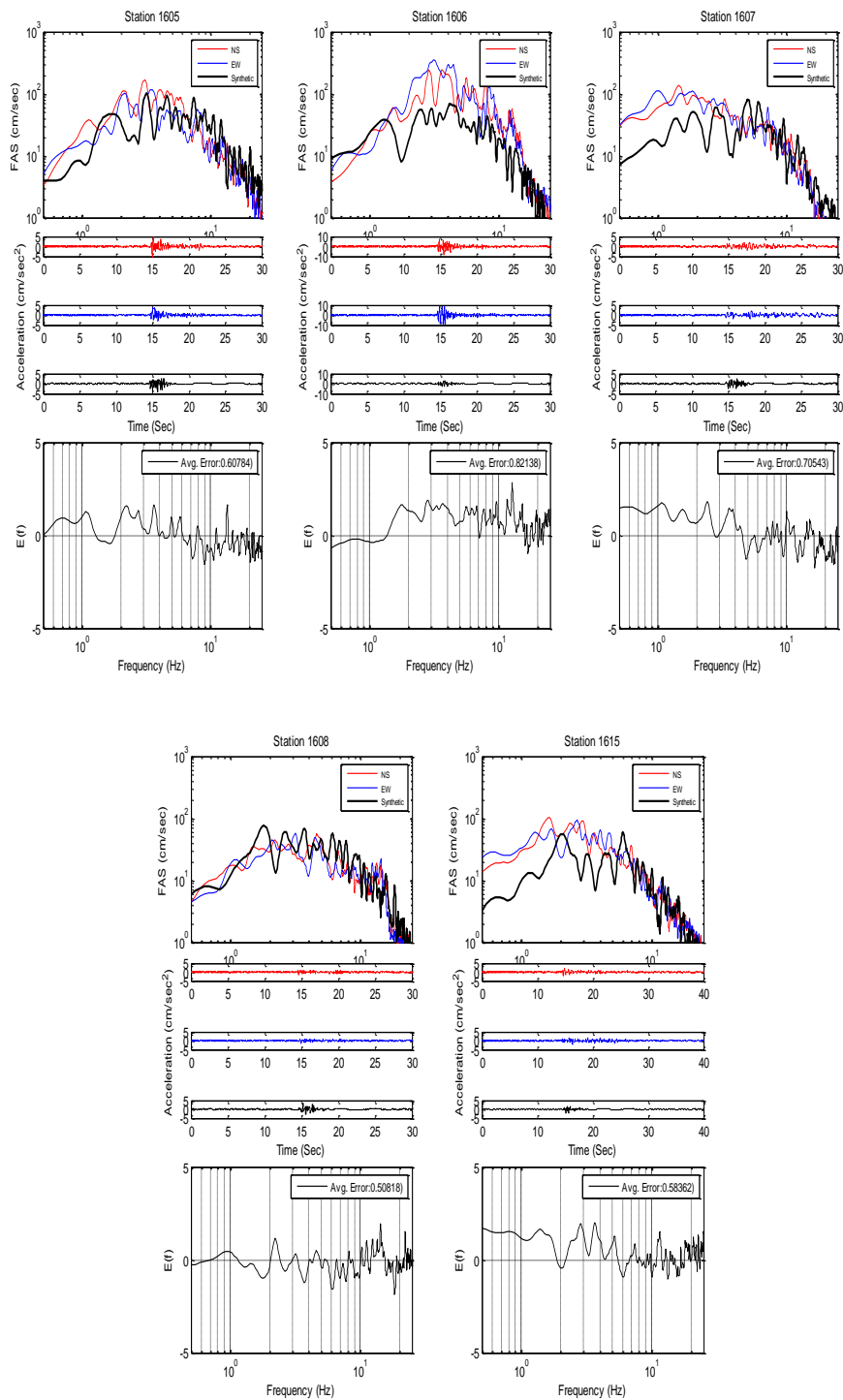


Figure 3.17 Comparison of Observed and Simulated Records for M.Kemalpassa Earthquake

For M.Kemalpassa earthquake, simulations yield accurate estimations for station 1605 and 1608 in both time and frequency domains. Even the source characteristics

at these stations are modeled accurately. At station 1606, simulated amplitudes at low frequencies match with those of the observed records. However, between 1Hz and 10Hz there is a clear underestimation of spectral amplitudes in the synthetic record as compared to the observed one. Lack of a clear S-wave pulse at station 1606 caused this issues. At station 1607 and 1615, the high frequency content matches with those of observed records. In both synthetics there is an underestimation until 3Hz. However, the misfits are less in the frequency band that is important in terms of engineering.

### **3.7 Comparison of Synthetics and Ground Motion Prediction Equations and Observations**

In order to further validate the simulations, the simulated motions in Bursa are compared with the recent ground motion equations. Among many ground motion prediction equations available in the literature, one regional (Akkar and Cagnan, 2010) and one global (Boore and Atkinson 2008) model are selected for comparisons. Comparisons are conducted with simulations at 500 dummy stations located in Bursa region for scenario events with  $M_w = 5$  to  $M_w = 7$  with magnitude intervals of  $\Delta M_w = 0.5$ . Fault dimensions are obtained by Wells and Coppersmith (1994) tables. The comparisons are performed assuming generic soil conditions ( $V_{s30}=310\text{m/s}$ ) at the nodes; this  $V_{s30}$  value is also used in the GMPEs. The comparisons for PGA, PGV and spectral accelerations for  $T=0.3, 1$  and  $2$  sec are presented in Figures 3.18-3.22.

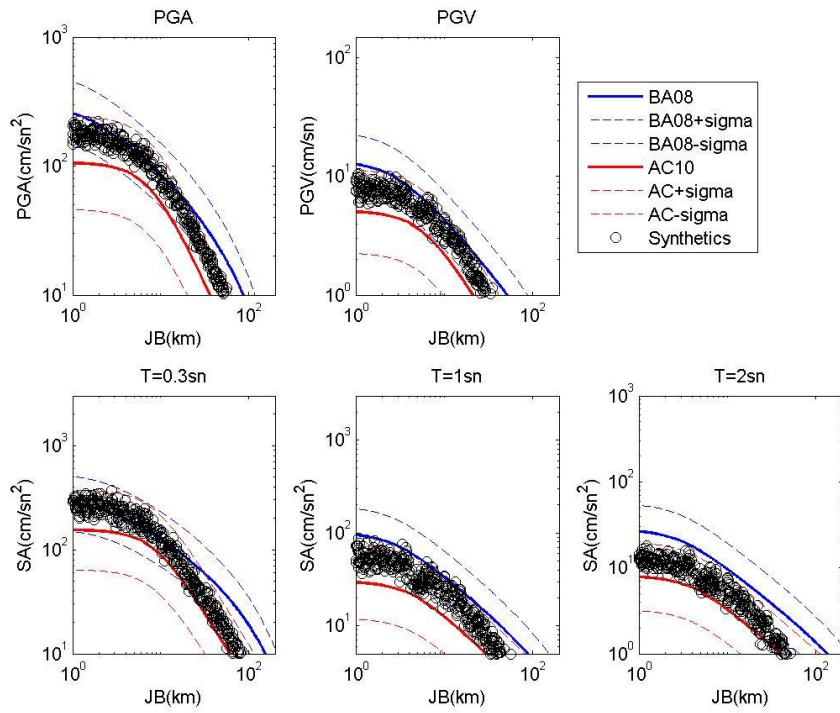


Figure 3.18 GMPE comparisons for Mw=5

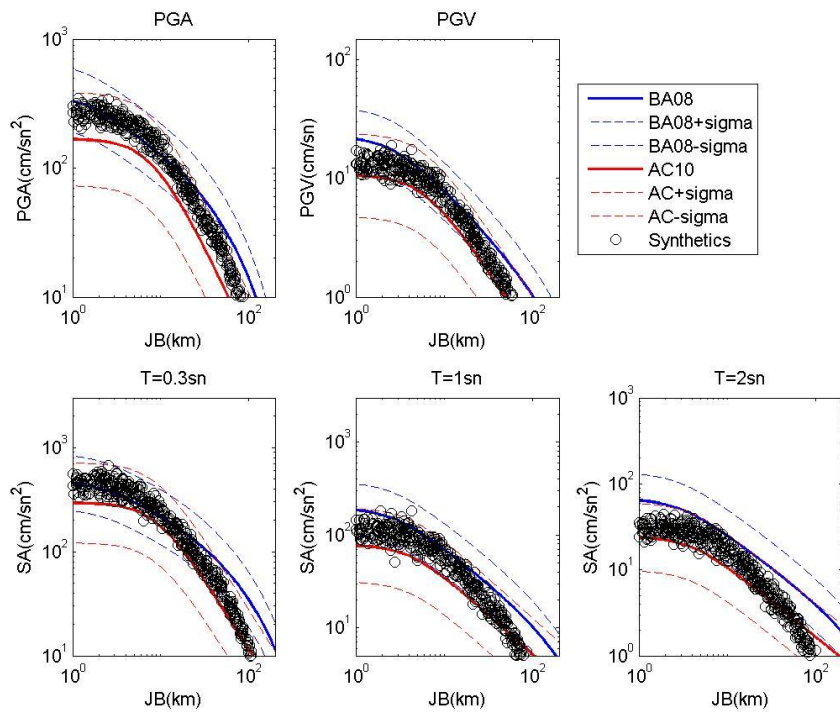


Figure 3.19 GMPE comparisons for Mw=5.5

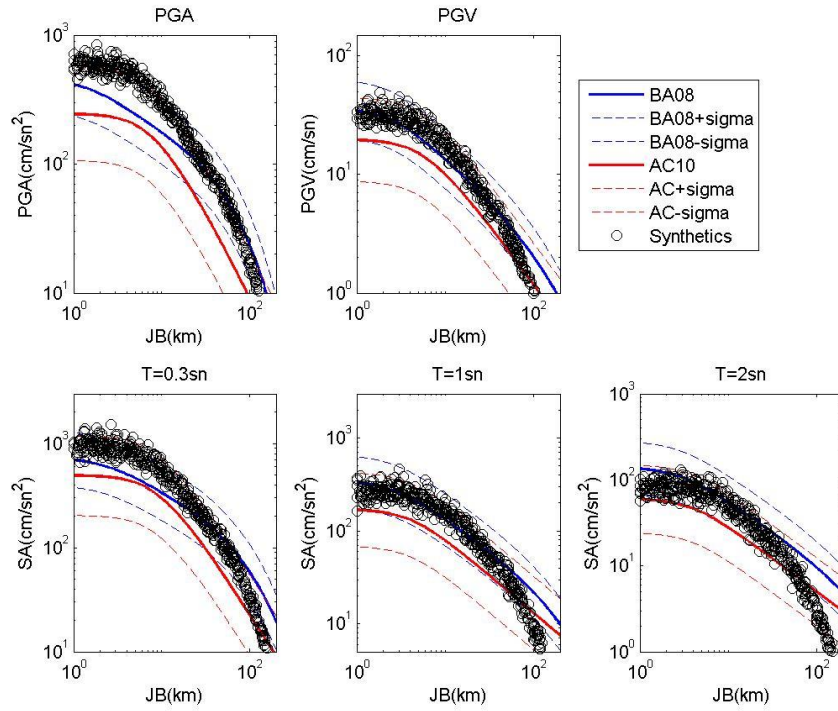


Figure 3.20 GMPE comparisons for Mw=6

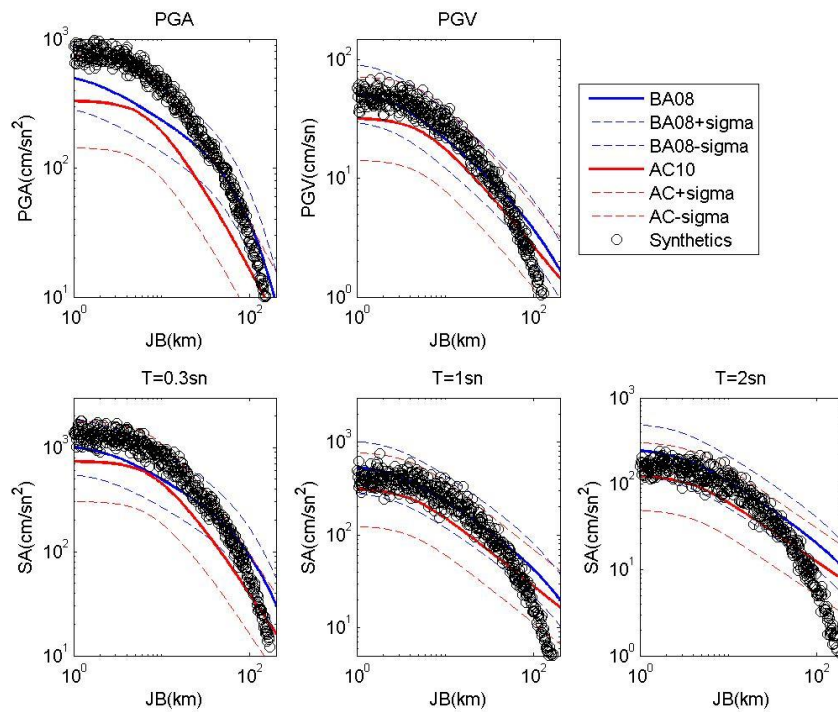


Figure 3.21 GMPE comparisons for Mw=6.5

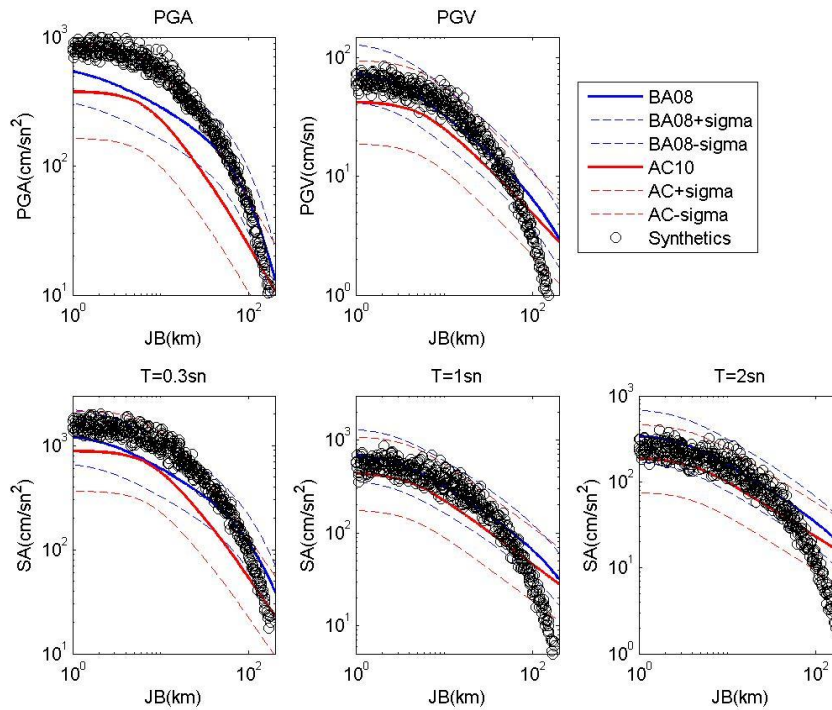


Figure 3.22 GMPE comparisons for Mw=7

It is observed that the synthetics are within  $\pm 1 \sigma$  of the ground motion prediction equations, especially for the smaller events. The major difference between the attenuation of synthetics and the ground motion prediction equations is for the data from large events at close distances, where the global data set for the GMPEs is well known to be limited. For PGA, the decay of simulated data at large distances matches that of GMPEs. Yet for the other parameters, some difference is observed which is believed to originate from the fact that the GMPEs cannot fully represent the regional path effects.

Overall, the comparison of the simulated data with observations and GMPEs reveals that the Bursa model is well-constrained and yields physically meaningful synthetic dataset. Thus, these model parameters will be used in the next Chapter to estimate the ground motion distribution from a potential scenario event in Bursa.

## **CHAPTER 4**

### **SCENARIO EARTHQUAKE ON BURSA FAULT AND INSURANCE IMPLICATIONS**

#### **4.1. Components of Earthquake Insurance**

Insurance is the risk sharing mechanism for disasters. Stakeholders must share the risk for healthy recovery after a catastrophic event. In order to distribute the risk fairly, the probability of loss caused by the catastrophic event must be known. Seismic risk of a region is the combination of seismic hazard and vulnerability in that region.

Knowledge of return periods of possible earthquakes and their magnitudes is crucial for insurance premium calculations. Return periods are obtained from seismological and geophysical studies. Vulnerability of any region can be measured by the degree of the observed damage after an earthquake. Damage assessment methods mostly categorize the damage states of structures ranging from no damage to collapse states.

Seismic hazard studies consider rupture possibility of every fault relevant to a site. Within the framework of Turkish Catastrophe Insurance Scheme, first, data obtained from seismic hazard analyses are combined with the vulnerability data. Then, insurance premiums are calculated based on the annual expected loss. In this study, only one scenario earthquake is considered and insurance premiums for that case are calculated.

In this chapter, first the scenario event will be presented followed by the description of the current insurance practice in Turkey and calculations.

## **4.2. Bursa Fault Scenario**

In Chapter 3, stochastic finite-fault simulation model for Bursa region is verified with past earthquakes and ground motion prediction equations. Synthetic ground motions at a site from a specific scenario earthquake can be generated from this model. Since the seismic hazard contribution of Bursa Fault is larger than other sources in the Bursa region based on Poisson model (Ozturk, 2008), an earthquake scenario on Bursa Fault generating its characteristic magnitude ( $M_W = 7.2$ ) is considered in this study. This event has a return period of 1000 years (Ozturk, 2008). Bursa Fault is a 45 km right lateral strike slip fault with normal component. It is located between Ulubat Lake and Bursa City in east-west direction (Topal et al., 2003). In the simulations, it is assumed that the rupture starts to propagate from the center of the fault.

In order to observe the effects of the fault rupture, 2025 dummy nodal points are selected around Bursa City Center (40.24° N, 29.08° E). Since not every nodal point has a soil profile or a detailed velocity model, observation points are divided into two groups with respect to site conditions at nearby stations. Site conditions are assumed to be similar to those at station 1608 for southern Bursa and station 1605 for northern Bursa. Parameter set used in the simulations is presented in Table 4.1 while the distribution of the peak ground motion acceleration values for the scenario event are shown in the Figure 4.1. Larger PGA values are observed especially in central and eastern Bursa. The largest PGA value is estimated as 1.037g, located to the northwest of the hypocenter due to the directivity effects.

Table 4.1 Parameter set utilized for Bursa scenario earthquake

Parameters	Values
Mw	7.2
Latitude of upper edge of fault (N)	40.2
Longitude of upper edge of fault (E)	29.03
Depth from surface (km)	7
Strike	103
Dip	90
Fault dimensions	45m x 25.5m
Subfault dimensions	0.5m x 0.5m
Crustal shear wave velocity(km/s)	3.5
Crustal density (g/cm <sup>3</sup> )	2.8
Rupture velocity(km/s)	2.8
Stress drop (bar)	118.75
Pulsing Area percent	50
Quality factor	$50f^{1.09}$
Geometric spreading	$R^{-1}, R \leq 30 \text{ km}$ $R^{-0.6}, 30 \text{ km} < R \leq 100 \text{ km}$ $R^{-0.5}, 100 \text{ km} < R$
Duration model	$T = T_0 + 0.05R$
Windowing function	(Saragoni and Hart 1973)
Kappa factor	Site specific $\kappa_0$
Site amplification factor	(Boore and Joyner, 1997)

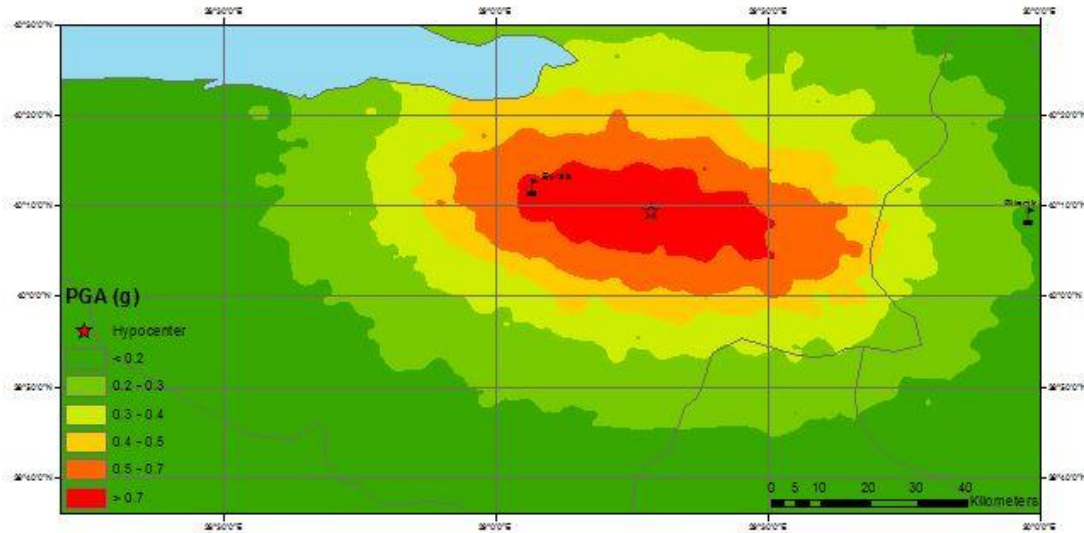


Figure 4.1 Peak ground acceleration distribution around Bursa City for Mw=7.2 scenario earthquake

For the damage estimation in this study, seismic intensity values in terms of Modified Mercalli Intensity (MMI) scale are required. Bilal and Askan (2014) developed empirical formulas to convert PGA and PGV to MMI as follows:

$$\begin{aligned}
 MMI &= 0.132 + 3.884 \times \log(PGA) \\
 MMI &= 2.673 + 4.340 \times \log(PGV)
 \end{aligned}
 \tag{4.1}$$

MMI distribution of the scenario event is presented in Figure 4.2. It can be observed that intensities IX and above IX dominate the region. This points out to the seismic vulnerability of the Bursa city center and the surrounding areas.

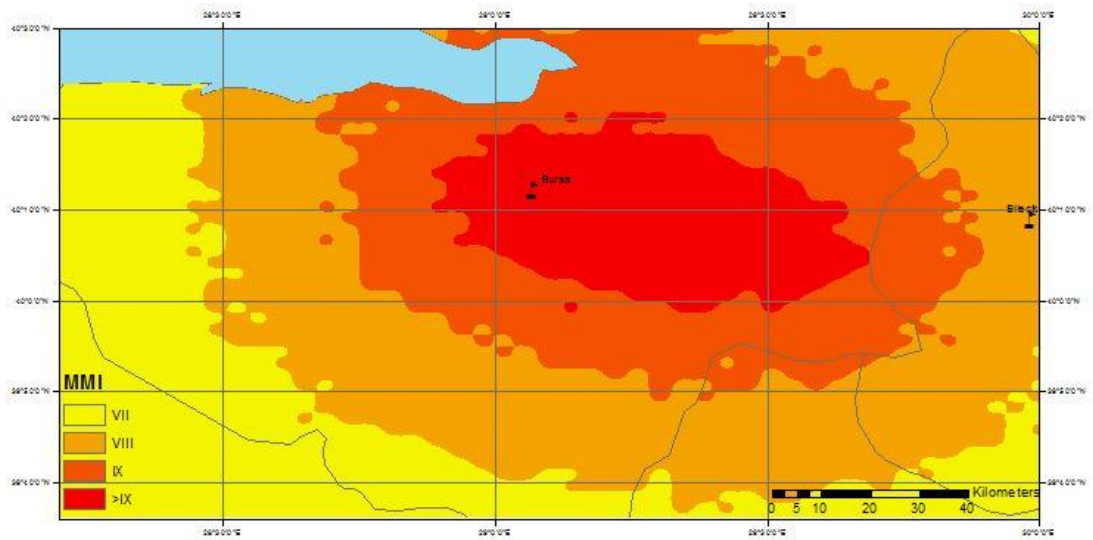


Figure 4.2 Distribution of MMI corresponding to the Mw=7.2 scenario earthquake around Bursa City

### 4.3. Earthquake Insurance Practice

Earthquakes have catastrophic outcomes. Combined with the inherent uncertainties involved, it is very difficult to provide affordable premium rates in earthquake insurance practice. Some portion of the uncertainties are caused by randomness of the earthquake itself, however lack of complete and proper information also cause uncertainties for earthquake insurance practice. Since the related information is not complete, there exists multiple methods for estimating damage and earthquake premiums. Provider of earthquake insurance in Turkey, Turkish Catastrophe Insurance Pool (TCIP), purposely underestimates the risk in order to guarantee minimum risk requirements and satisfying economical premiums under lack of proper information.

TCIP was established as a legal entity after catastrophic Düzce and Kocaeli earthquakes in 1999 and started operating in September 2000. TCIP is responsible for providing and managing Compulsory Earthquake Insurance in Turkey. Main purpose of TCIP is to reduce the immediate economic impact of earthquakes to government and building long-term reserves for financing future earthquakes. Increasing the earthquake insurance penetration rates is one of the main goals of

TCIP, therefore earthquake insurance to residential buildings are provided with low premium rates (Gurenko, 2006). In 1999, earthquake insurance was offered as an optional endorsement to the fire policy and the penetration rate for it was 4.6% (Gurenko, 2006). Currently, 7.2 million households are insured which corresponds to penetration rate of 40.8%. Yearly number of premiums and their values are tabulated in Table 4.2. There is an increasing trend for both number of premiums and total premium value.

Table 4.2 Yearly premium number and total premium values (TCIP, 2015)

Year	Number of premiums (10 <sup>6</sup> )	Increase in number (%)	Total premium value (10 <sup>6</sup> TL)	Increase of total premium value (%)
27/09-31/12/200	159	-	3.766	-
2001	2.428	-	54.526	-
2002	2.128	-12.40	65.756	20.60
2003	2.022	-5.00	85.688	30.30
2004	2.090	-3.40	126.216	47.30
2005	2.417	15.60	159.085	26.00
2006	2.555	5.70	205.799	29.40
2007	2.618	2.50	234.615	14.00
2008	2.844	8.60	272.637	16.20
2009	3.435	20.80	322.065	18.10
2010	3.316	-3.50	319.415	-0.80
2011	3.725	12.30	378.782	18.60
2012	4.786	28.50	509.771	34.60
2013	6.029	26.00	674.140	32.20
2014	6.808	12.90	753.909	11.80

Earthquake risk in Turkey is shared globally by reinsuring of the TCIP. Two of the TCIP's reinsurers are Swiss Re and Munich Re. Swiss Re, founded in 1863, is one of the leading global reinsurance companies. This company reinsured TCIP for USD 100m recently (Swiss Re, 2015). This catastrophe bond complements the existing reinsurance program and provides three-year coverage. The bond has a parametric trigger. When the predetermined earthquake conditions are met, TCIP is paid immediately. The company also supports the existing reinsurance program (Swiss Re, 2015). Munich Re is founded in 1880, is one of the lead supporter of TCIP with

USD 400m catastrophe bond. This bond is reinsurance protection for earthquake risks in Turkey with a statistical return period of around one event per 100 years.

TCIP calculates the earthquake insurance premiums using three components; earthquake zone according to the Turkish Earthquake Zonation Map, structural type and m<sup>2</sup> of the dwelling. There are 15 tariff rates for 3 structural types and 5 earthquake zones (Table 4.3). Earthquake insurance premiums are calculated by multiplying tariff rate with the insured sum (unit price of the building times m<sup>2</sup>). However, the factors including the hazard state before and after the earthquakes, the dwelling specifics such as number of floors, age and some other incorporating factors are not incorporated into the premium valuation.

Table 4.3 Earthquake insurance premium rates for Turkey (TCIP, 2015)

Structural Type	Zone 1	Zone 2	Zone 3	Zone 4	Zone 5
1. Steel, reinforced concrete	2.20‰	1.55‰	0.83‰	0.55‰	0.44‰
2. Masonry	3.85‰	2.75‰	1.43‰	0.60‰	0.50‰
3. Other	5.50‰	3.53‰	1.76‰	0.78‰	0.58‰

#### 4.4. Damage Probability Matrices for Turkey

TCIP uses a seismic zonation map, therefore in the insurance premium calculations all possible earthquakes caused by nearby faults are taken into account. In this study, a scenario earthquake on Bursa Fault is studied and insurance premiums only for that event are calculated. Insurance premiums are calculated with three methods in this thesis: (i) probabilistic model for the estimation of earthquake insurance premiums proposed by Yucemen (2005), (ii) loss level methodology presented by Kanda and Nishijima (2004) and (iii) loss generation with respect to lognormal distribution that utilizes probabilistic model (Yucemen, 2005) with a new damage probability matrix (DPM) generated from damage simulations in this study.

Damage probability matrices are used to estimate the vulnerability of a specific structural type under various levels of seismic intensity. Seismic damage has major

uncertainties involved, therefore it should be represented in a probabilistic framework. An element in the damage probability matrix (DPM),  $P(DS,I)$ , is the probability of occurrence of damage state  $DS$  under seismic intensity  $I$ . Probabilities of damage states for each intensity naturally adds up to 1. Intensity is generally represented in terms of MMI. Ground motion parameters can also be used as intensity parameter. However, since historical damage data is in terms of MMI and often other ground motion parameters are not known in such old data, mostly MMI is used in DPMs.

Damage states in DPMs are qualitative damage states for a specific structural type. In Turkey, they range from None to Collapse. The damage states have also quantitative values for mathematical representations. These quantitative values are mostly possible damage ranges, because even for the same structural type, damage can vary according to soil conditions and structural layout. For computational purposes, these damage ranges are represented with a single mean value named as Central Damage Ratio (CDR). The correlation between damage states and damage ratios depends on the design regulations in a country. In Turkey, qualitative damage states are specified as None (N), Light Damage (L), Moderate Damage (M), Heavy Damage (H) and Collapse (C). The damage ratios and CDRs corresponding to different damage states as estimated by Gurpinar et al. (1978) are shown in Table 4.4.

Table 4.4 Central damage ratios for damage states Gurpinar et al. (1978)

Damage State (DS)	Damage Ratio (DR) %	Central Damage Ratio (CDR) %
None	0-1	0
Light	1-10	5
Moderate	10-50	30
Heavy	50-90	70
Collapse	90-100	100

In insurance premium calculations for each MMI level, probabilities of each damage state is multiplied by the CDR of that damage state and summed up in order to obtain a single expected damage ratio or mean damage ratio (MDR).

Earlier DPMs for Turkey were developed by Gurpinar et al. (1978) as shown in Table 4.5. In this study, expert opinions are used to estimate damage state probabilities due to the limited amount of data from previous earthquakes. These DPMs have two sets of damage probabilities: According to Code (AC) set represents structures designed and constructed with respect to the earthquake specifications. In the other set, structures are assumed to be not designed and constructed according to the code specifications (NAC).

Table 4.5 Damage probability matrix proposed by Gurpinar et al. (1978)

Damage State	CDR(%)	MMI V		VI		VII		VIII		IX	
		AC	NAC	AC	NAC	AC	NAC	AC	NAC	AC	NAC
None	0	1.0	0.95	0.95	0.70	0.70	0.50	0.50	0.20	0.30	0.05
Light	5	0	0.05	0.05	0.15	0.20	0.20	0.20	0.20	0.30	0.20
Moderate	30	0	0	0	0.10	0.10	0.15	0.20	0.40	0.20	0.40
Heavy	70	0	0	0	0.05	0	0.10	0.10	0.10	0.20	0.20
Collapse	100	0	0	0	0	0	0.05	0	0.10	0	0.15
MDR (%)		0	0.25	0.25	7.25	4	17.5	14	30	21.5	42

Yucemen and Bulak (1997) proposed new DPM's using the damage statistics obtained from major earthquakes that occurred after Gurpinar et al.'s (1978) study.

In the recent study by Askan and Yucemen (2010), 4 major earthquakes (1995 Dinar, 1998 Ceyhan, 1999 Marmara and 1999 Duzce) are also incorporated to the data from Gurpinar et al. (1978) and Yucemen and Bulak (1997) studies. Empirical damage reports were employed for these earthquakes in Askan and Yucemen (2010). Weighted average of expert opinion and empirical damage reports were used for estimating the DPM's for Zone 1 and Zone 2. In this thesis, DPM proposed in Askan and Yucemen (2010) for Zone 1 is used in insurance premium calculations (Table 4.6).

Table 4.6 Damage probability matrix for Zone 1 (Askan and Yucemen, 2010)

Damage State	CDR(%)	MMI									
		V		VI		VII		VIII		IX	
		AC	NAC	AC	NAC	AC	NAC	AC	NAC	AC	NAC
None	0	1.0	0.95	0.95	0.58	0.70	0.46	0.50	0.28	0.30	0.07
Light	5	0	0.05	0.05	0.29	0.20	0.34	0.20	0.39	0.30	0.27
Moderate	30	0	0	0	0.11	0.10	0.14	0.20	0.20	0.20	0.30
Heavy	70	0	0	0	0.02	0	0.05	0.10	0.07	0.20	0.19
Collapse	100	0	0	0	0	0	0.01	0	0.06	0	0.17
MDR (%)		0	0.25	0.25	6.2	4	10.4	14	18.9	21.5	40.7

#### 4.5. Valuation of the Earthquake Insurance Premium

In this section, three alternative approaches are employed and compared with previous studies. These methods are:

- i. Probabilistic model for the estimation of earthquake insurance premiums
- ii. Loss level method
- iii. Loss generation with respect to lognormal distribution

##### i. Probabilistic Model for the Estimation of Earthquake Insurance Premiums

In this method, pure premium is calculated in terms of expected annual damage ratio (*EADR*) proposed by Yucemen (2005) as:

$$EADR_k = \sum_I MDR_k(I) \times SH_I \quad (4.2)$$

where *SH* is the seismic hazard term which is the annual probability of an earthquake with intensity *I* and *MDR(I)* is the mean damage ratio of an earthquake with intensity *I*. *MDR* for each intensity level is calculated as:

$$MDR_k(I) = \sum_{DS} P_k(DS, I) \times CDR_{DS} \quad (4.3)$$

where  $CDR$  and  $P(DS, I)$  are as defined previously.

Pure risk premium ( $PRP$ ) is calculated as:

$$PRP_k = EADR_k \times INSV \quad (4.4)$$

where  $INSV$  is the insured value of the building. Using the seismic hazard term related to Bursa Fault as 1/1000 (Ozturk, 2008), the pure risk premium ( $PRP$ ) is estimated in Table 4.7.

Table 4.7 Pure risk premiums calculated from Askan and Yucemen (2010) DPM

Damage State	CDR(%)	MMI V		VI		VII		VIII		IX	
		AC	NAC	AC	NAC	AC	NAC	AC	NAC	AC	NAC
None	0	1.0	0.95	0.95	0.58	0.70	0.46	0.50	0.28	0.30	0.07
Light	5	0	0.05	0.05	0.29	0.20	0.34	0.20	0.39	0.30	0.27
Moderate	30	0	0	0	0.11	0.10	0.14	0.20	0.20	0.20	0.30
Heavy	70	0	0	0	0.02	0	0.05	0.10	0.07	0.20	0.19
Collapse	100	0	0	0	0	0	0.01	0	0.06	0	0.17
MDR (%)		0	0.25	0.25	6.2	4	10.4	14	18.9	21.5	40.7
EADR (‰)		0	0.0025	0.0025	0.062	0.04	0.104	0.14	0.189	0.215	0.407
PRP (‰*INSV)		0	0.0025	0.0025	0.062	0.04	0.104	0.14	0.189	0.215	0.407

It is observed that the NAC structures experience considerably higher damage than AC structures do. Moreover, the difference in MDR is more significant for higher intensities. This is expected since, for instance, NAC structures have 34% chance to survive an event with  $MMI = 9$  with less than moderate damage, whereas this value increases to 60% for AC structures.

## ii. Loss Level Method

According to this methodology, there are three loss levels and a proportion of the insured value is paid according to these levels. Qualitative representations of the

damage states are different than those in Turkey. These damage states are converted into Turkish ones according to their CDR. According to new damage state representations, none and light damage are combined and represented by slight damage. Moderate, heavy and collapse damage states are represented by moderate, severe and collapse states respectively. After the conversion, first loss level (L1) includes none and light damage states. Second loss level (L2) includes moderate and heavy damage states. Third loss level (L3) corresponds to the collapse state. Kanda and Nishijima (2004) proposed that 5%, 50% and 100% of the insured value is paid for L1, L2 and L3 respectively, as follows:

$$\begin{aligned}
 L1 &= SH \times P(Slight) \times 0.05 \\
 L2 &= SH \times (P(Moderate) + P(Severe)) \times 0.5 \\
 L3 &= SH \times P(Collapse) \times 1
 \end{aligned} \quad (4.5)$$

Pure risk premium is calculated as follows:

$$PRP = (L1 + L2 + L3) \times INSV \quad (4.6)$$

Using the damage state probabilities in DPM for Zone 1 (Askan and Yucemen, 2010), probabilities for Kanda and Nishijima (2004) damage states are estimated in Table 4.8. The corresponding pure risk premiums are presented in Table 4.9.

Table 4.8 Modified DPM with respect to loss level method

Damage State	MMI V		VI		VII		VIII		IX	
	AC	NAC	AC	NAC	AC	NAC	AC	NAC	AC	NAC
Slight	1	1	1	0.87	0.90	0.80	0.70	0.67	0.60	0.34
Moderate	0	0	0	0.11	0.10	0.14	0.20	0.20	0.20	0.30
Severe	0	0	0	0.02	0	0.05	0.10	0.07	0.20	0.19
Collapse	0	0	0	0	0	0.01	0	0.06	0	0.17

Table 4.9 Pure risk premiums with respect to loss level method

Loss Level	MMI									
	V		VI		VII		VIII		IX	
	AC	NAC	AC	NAC	AC	NAC	AC	NAC	AC	NAC
L1 (‰)	0.05	0.05	0.05	0.0435	0.045	0.04	0.035	0.0335	0.03	0.017
L2 (‰)	0	0	0	0.065	0.05	0.095	0.15	0.135	0.2	0.245
L3 (‰)	0	0	0	0	0	0.01	0	0.06	0	0.17
PRP(‰*INSV)	0.05	0.05	0.05	0.1085	0.095	0.145	0.185	0.2285	0.23	0.432

Similarly, differences in pure risk premiums for AC and NAC buildings at higher intensities are observed with this method. In this case, the premiums for L1 and L2 are similar, while premium for NAC structures is significantly higher for L3, and this premium for L3 is almost equal to the total *PRP* difference between AC and NAC buildings.

### iii. Loss Generation with respect to Lognormal Distribution

Inspired by the flood damage simulations performed by Paudel et al. (2013), earthquake damage is simulated for Bursa. Damage states are assumed to have lognormal distribution similar to the approach by Kanda and Nishijima (2004). Covariances for each MMI are estimated using DPMs in Askan and Yucemen (2010) study. Building information in Bursa were not available. Therefore, for each MMI, damage states of one million arbitrary reinforced concrete structures are simulated. Simulations are repeated twice, assuming both AC and NAC conditions for all buildings. With the simulated damage state probabilities a new DPM is formed. The approach by Yucemen (2005), as described in (i), is employed for this new DPM.

MATLAB is utilized to generate lognormally distributed random numbers for the damage simulations. Input parameters of lognormal random number generator function (*logrnd*) are  $\mu$  and  $\sigma$ . For each MMI, these parameters are calculated as follows:

$$\mu = \log\left(CDR^2_{DS}/\sqrt{\sigma^2_{MMI} + CDR^2_{DS}}\right)$$

$$\sigma = \sqrt{\log(\sigma^2_{MMI}/CDR^2_{DS} + 1)} \quad (4.7)$$

where

$$\sigma^2_{MMI} = \sum_{DS} P(DS) \times (MDR_{MMI} - CDR_{DS})^2 \quad (4.8)$$

Damage is computed as follows:

$$\pi = E(Loss) + \frac{\sigma^2 \times r}{2} \quad (4.9)$$

where  $r$  is the adjustment coefficient and taken as  $r=0.005$  (Kaas et al., 2008).

After the damage simulations, a new DPM is generated and tabulated in Table 4.10.

Table 4.10 DPM generated from damage simulations

Damage State	CDR(%)	MMI									
		V		VI		VII		VIII		IX	
		AC	NAC	AC	NAC	AC	NAC	AC	NAC	AC	NAC
None	0	1	0.95	0.95	0.22	0.35	0.10	0.03	0.01	0	0
Light	5	0	0.05	0.05	0.62	0.56	0.62	0.57	0.46	0.37	0.07
Moderate	30	0	0	0	0.14	0.08	0.25	0.36	0.45	0.54	0.67
Heavy	70	0	0	0	0.01	0	0.02	0.03	0.05	0.06	0.18
Collapse	100	0	0	0	0	0	0.01	0.01	0.02	0.02	0.08
MDR (%)		0	0.28	0.28	8.32	5.68	12.98	17.02	21.65	24.78	40.96

Based on the generated DPMs, pure risk premiums are calculated and presented in Table 4.11.

Table 4.11 Pure risk premium calculated by using the DPM generated from damage simulations

	MMI									
	V		VI		VII		VIII		IX	
	AC	NAC	AC	NAC	AC	NAC	AC	NAC	AC	NAC
MDR (%)	0	0.28	0.28	8.32	5.68	12.98	17.02	21.65	24.78	40.96
EADR (‰)	0	0.0028	0.0028	0.0832	0.0568	0.1298	0.1702	0.2165	0.2478	0.4096
PRP (‰*INSV)	0	0.0028	0.0028	0.0832	0.0568	0.1298	0.1702	0.2165	0.2478	0.4096

Damage simulations and Askan and Yucemen (2010) DPM yields very similar results. This could prove that the damage states are lognormally distributed.

#### 4.6. Comparison of the Premium Calculation Methods

For a single deterministic scenario earthquake, insurance premiums are calculated using three different methods. It can be observed in Table 4.12 that probabilistic model and loss generation method yields similar results. Estimations from loss level method are slightly higher than the other two methods above the intensity level of VII.

Table 4.12 Comparison of pure premiums with respect to three models

PRP method	MMI									
	V		VI		VII		VIII		IX	
	AC	NAC	AC	NAC	AC	NAC	AC	NAC	AC	NAC
Probabilistic model (‰)	0	0.0025	0.0025	0.062	0.04	0.104	0.14	0.189	0.215	0.407
Loss level method (‰)	0.05	0.05	0.05	0.1085	0.095	0.145	0.185	0.2285	0.23	0.432
Loss generation method (‰)	0	0.0028	0.0028	0.083	0.057	0.130	0.17	0.217	0.248	0.410

Direct comparison with the TCIP is not possible, because the TCIP premium rates are estimated according to probabilistic seismic hazard analyses whereas in this study only one of the hazard scenarios is considered. However, for verification, the results of this thesis are compared to those of Ekici (2015), who calculated earthquake premiums for Istanbul. In Ekici (2015), new representative fragility curves for reinforced concrete and masonry buildings are suggested based on fragility curves in previous studies. Insurance premium rates are then calculated from these fragility curves for return periods of 75 years, 475 years and 2475 years in terms of MMI. Then, these insurance premium rates are compared with the TCIP premium rates. In that study, it is observed that the TCIP premium rates lie between maximum and average of the computed premium rates for the given return periods.

TCIP uses a loading factor of  $\theta^{-1} = 1.097$  which is also used in the Ekici (2015). When multiplied with the loading factor, gross premiums are obtained and presented in Table 4.13.

Table 4.13 Gross premium with respect to three models

PRP method	MMI V		VI		VII		VIII		IX	
	AC	NAC	AC	NAC	AC	NAC	AC	NAC	AC	NAC
	Probabilistic model (‰)	0	0.0027	0.0027	0.0680	0.0439	0.1141	0.1536	0.2073	0.2359
Loss level method (‰)	0.0549	0.0549	0.0549	0.1190	0.1042	0.1591	0.2029	0.2507	0.2523	0.4739
Loss generation method (‰)	0.0000	0.0030	0.0030	0.0912	0.0623	0.1424	0.1867	0.2375	0.2719	0.4493

In Ekici (2015), for low rise and mid-rise reinforced concrete type buildings premium rates for return period 2475 years at earthquake Zone 1 are between 0.2‰ and 0.25‰. The premium rates for buildings designed and constructed according to code at the intensity level IX are estimated also to be in the range of 0.2‰ to 0.25‰ in this study. Thus, the premium rates in Ekici (2015), for a return period of 2475 years is found to be similar to premium rates computed herein for a single event with a return period of 1000 years. This observation seems to be reasonable.

## CHAPTER 5

### CONCLUDING REMARKS

#### 5.1 Summary

Simulations are effective tools for generating ground motion records for regions with no or sparse seismic networks. They provide amplitude and frequency content as well as acceleration time histories of ground motions from past or potential earthquakes. Simulations are also essential for cases where peak ground motion parameters are not sufficient and full time histories of the records are required. Simulation outputs have been utilized for many earthquake engineering applications ranging from seismic hazard assessment to earthquake resistant design. Moreover, simulations also give insight over the regional seismic parameters.

In this study, past earthquakes in Bursa region as well as a scenario event are simulated based on stochastic finite-fault simulation with dynamic corner frequency model. This method is a practical and accurate option for simulating high frequency portions of shear-waves. Accuracy of the simulation models directly depend on the parameter selection. In this study, parameters are either derived from regional data or adapted from previous studies in Bursa region.

Initially, Bursa simulation model is prepared using regional parameters. Then this model is verified with 4 past earthquakes that occurred in Bursa region. The optimized simulation model is compared with one global and one regional GMPE.

Next, using the verified model, a potential deterministic scenario is simulated and spatial distribution of the corresponding peak ground motion parameters is studied. Then, peak ground accelerations of this scenario event are converted to MMI values in the region. Through DPMs, these MMIs are then converted to CDRs. Using previous seismic hazard studies, return period of the scenario event is obtained. Insurance premiums are calculated with three alternative techniques using seismic hazard parameters and MDRs.

## **5.2 Observations and Conclusions**

Detailed observations and conclusions of this study are as follows:

- This study constitutes a first attempt to study past and potential events in Bursa region using ground motion simulations.
- Using carefully selected regional input parameters stochastic simulations yield accurate strong ground motion estimations of observed events. These input parameters and results of simulations are available for use in other studies in the future.
- Stochastic finite-fault simulation with dynamic corner frequency method has limited accuracy for low frequency range ( $<1\text{Hz}$ ) due to the absence of the source complexities and full wave propagation solution.
- Path parameters are especially effective for simulations at distant locations from the sources. In particular, frequency-dependent quality factor can alter the amplitude and frequency content of the simulated ground motions completely. It is crucial to utilize a quality factor representing regional (path) attenuation properties.
- Site parameters also have major impact on the amplitudes, duration and frequency content of the simulated time series. Therefore, accurate assessment of local site conditions is essential for reliable simulations.

- For regions where the regional parameters inherit high uncertainty due to lack of complete regional datasets, simulation models must be validated with previous earthquakes.
- Strong ground motion records from simulations of small to moderate earthquakes result in close matches with the available GMPEs. However, for events with  $M_w > 6$ , GMPEs and simulations yield different results most probably due to lack of data at close distances for large events.
- Stochastic simulations are effectively used to predict spatial distributions of ground motions and intensity values caused by a potential earthquake scenario.
- Three different premium calculation approaches based on the same DPM yields similar results. Thus, the structural damage models are very significant in insurance premium calculations and must be studied carefully.
- Insurance premiums for an event with 1000 year return period is observed to be comparable to insurance premiums computed from regional seismic hazard analysis for 2475 year return period.
- By modeling the physics of ground motion generation process, insurance premium rates can be computed for regions with sparse data from large events.

### **5.3 Future Recommendations**

Based on the conclusions of this thesis, following are the recommendations for future similar studies:

- Due to inherent limitations of stochastic simulations at lower frequencies, stochastic simulations must be combined with deterministic simulations in

order to obtain reliable broadband ground motions. To employ these hybrid methods, well-resolved wave velocity models of the area of interest must be available.

- Simulations require well-constrained input parameters for reliable results. Many input parameters in this study are derived from the recordings of the regional seismic network. Increasing the seismic network in seismically active regions will enhance the quality of the input parameters.
- Frequency-dependent path effects have direct impact on the amplitude and frequency content of the simulated ground motions. Studies on regional path parameters will improve the accuracy of the simulations.
- Site parameters affect the amplitude, duration and frequency content of the simulations. Increasing the number and density of boreholes as well as employing other site characterization studies for obtaining velocity profiles is crucial for obtaining theoretical site amplification factors. In addition, construction of kappa models for seismically active regions will reduce the effort required to determine site parameters during simulations.
- Damage models are crucial for insurance premium calculations. However, there is a trade-off between cost and reliability of the damage assessment methods. Also the structural damage data is mostly only available after large events. Thus, development of a robust damage model would increase the reliability of insurance premium calculations.
- Damage simulations based on regional building information such as building type, building being AC or NAC and number of buildings, would yield more realistic results.
- Insurance premium calculations based on probabilistic seismic hazard assessment studies are more comparable to TCIP. Therefore, simulation of

multiple events and to involve all cases in the premium calculations could increase the understanding of significance and sensitivity of insurance premium calculation parameters.



## REFERENCES

- Aki, K. (1967). Scaling law of seismic spectrum. *Journal of Geophysical Research*, 72(4), 1217.
- Aki, K., and Richards, P. G. (1980). *Quantative seismology: Theory and methods*. Vol II.
- Akinci, A., and Antonioli, A. (2013). Observations and stochastic modelling of strong ground motions for the 2011 October 23 Mw 7.1 Van, Turkey, earthquake. *Geophysical Journal International*, 192(3), 1217–1239.
- Akkar, S., and Çağnan, Z. (2010). A local ground-motion predictive model for Turkey, and its comparison with other regional and global ground-motion models. *Bulletin of the Seismological Society of America*, 100(6), 2978–2995.
- Akyol, N., Akıncı, A., and Eyidoğan, H. (2002). Site amplification of S-waves in Bursa City and its vicinity, northwestern Turkey: Comparison of different approaches. *Soil Dynamics and Earthquake Engineering*, 22(7), 579–587.
- Ambraseys, N. (2002). The seismic activity of the Marmara Sea region over the last 2000 years. *Bulletin of the Seismological Society of America*, 92(1), 1–18.
- Ambraseys, N. N. (2000). The Seismicity of the Marmara Sea Area 1800–1899. *Journal of Earthquake Engineering*, 4(3), 377–401.
- Anderson, J. G., and Hough, S. E. (1984). A model for the shape of the fourier amplitude spectrum of acceleration at high frequencies. *Bulletin of the Seismological Society of America*, 74(5), 1969–1993.
- Ansal, A., Akinci, A., Cultrera, G., Erdik, M., Pessina, V., Tönük, G., and Ameri, G. (2009). Loss estimation in Istanbul based on deterministic earthquake scenarios of the Marmara Sea region (Turkey). *Soil Dynamics and Earthquake Engineering*, 29(4), 699–709.
- Askan, A., Sisman, F. N., and Ugurhan, B. (2013). Stochastic strong ground motion simulations in sparsely-monitored regions: A validation and sensitivity study on the

13 March 1992 Erzincan (Turkey) earthquake. *Soil Dynamics and Earthquake Engineering*, 55, 170–181.

Askan, A., and Yucemen, M. S. (2010). Probabilistic methods for the estimation of potential seismic damage: Application to reinforced concrete buildings in Turkey. *Structural Safety*, 32(4), 262–271.

Atkinson, G. M. (2004). Empirical attenuation of ground-motion spectral amplitudes in southeastern Canada and the northeastern United States. *Bulletin of the Seismological Society of America*, 94(3), 1079–1095.

Atkinson, G. M., Assatourians, K., Boore, D. M., Campbell, K., and Motazedian, D. (2009). A guide to differences between stochastic point-source and stochastic finite-fault simulations. *Bulletin of the Seismological Society of America*, 99(6), 3192–3201.

Atkinson, G. M., and Silva, W. (2000). Stochastic modeling of California ground motions. *Bulletin of the Seismological Society of America*, 90(2), 255–274.

Beresnev, I. A., and Atkinson, G. M. (1997). Modeling finite-fault radiation from the  $\omega$ n spectrum. *Bulletin of the Seismological Society of America*, 87(1), 67–84.

Beresnev, I. A., and Atkinson, G. M. (1998). FINSIM--a FORTRAN Program for Simulating Stochastic Acceleration Time Histories from Finite Faults. *Seismological Research Letters*, 69(1), 27–32.

Bilal, M., and Askan, A. (2014). Relationships between Felt Intensity and Recorded Ground-Motion Parameters for Turkey. *Bulletin of the Seismological Society of America*.

Bonilla, L. F., Steidl, J. H., Gariel, J.-C., and Archuleta, R. J. (2002). Borehole response studies at the Garner Valley downhole array, southern California. *Bulletin of the Seismological Society of America*, 92(8), 3165–3179.

Boore, D. M. (1983). Stochastic simulation of high-frequency ground motions based on seismological models of the radiated spectra. *Bulletin of the Seismological Society of America*, 73(6), 1865–1894.

Boore, D. M. (1984). Use of seismoscope records to determine ML and peak velocities. *Bulletin of the Seismological Society of America*, 74(1), 315–324.

Boore, D. M. (2003). Simulation of Ground Motion Using the Stochastic Method. *Pure and Applied Geophysics*, 160(3), 635–676.

Boore, D. M. (2013). The Uses and Limitations of the Square-Root-Impedance Method for Computing Site Amplification. *Bulletin of the Seismological Society of America*, 103(4), 2356–2368.

Boore, D. M., and Atkinson, G. M. (2008). Ground-motion prediction equations for the average horizontal component of PGA, PGV, and 5%-damped PSA at spectral periods between 0.01 s and 10.0 s. *Earthquake Spectra*, 24(1), 99–138.

Boore, D. M., and Joyner, W. B. (1997). Site amplifications for generic rock sites. *Bulletin of the Seismological Society of America*, 87(2), 327–341.

Brune, J. N. (1970). Tectonic stress and the spectra of seismic shear waves from earthquakes. *Journal of Geophysical Research*, 75(26), 4997.

Brune, J. N. (1971). Correction. *Journal of Geophysical Research*, 76, 5002.

Castro, R. R., Pacor, F., Franceschina, G., Bindi, D., Zonno, G., and Luzi, L. (2008). Stochastic strong-motion simulation of the Mw 6 Umbria-Marche Earthquake of September 1997: Comparison of different approaches. *Bulletin of the Seismological Society of America*, 98(2), 662–670.

Castro, R. R., Rovelli, A., Cocco, M., Di Bono, M., and Pacor, F. (2001). Stochastic simulation of strong-motion records from the 26 September 1997 (Mw6), Umbria-Marche (Central Italy) earthquake. *Bulletin of the Seismological Society of America*, 91(1), 27–39.

Chiou, B. S.-J., and Youngs, R. R. (2014). Update of the Chiou and Youngs NGA model for the average horizontal component of peak ground motion and response spectra. *Earthquake Spectra*, 30(3), 1117–1153.

Ekici, M. A. (2015). Generalized Fragility Curves For Earthquake Insurance Premiums. Unpublished, Ms Thesis, METU

ESRI 2011. ArcGIS Desktop: Release 10. Redlands, CA: Environmental Systems Research Institute.

Field, E. H., and Jacob, K. H. (1995). A comparison and test of various site-response estimation techniques, including three that are not reference-site dependent. *Bulletin of the Seismological Society of America*, 85(4), 1127–1143.

Galluzzo, D., Zonno, G., and Del Pezzo, E. (2008). Stochastic finite-fault ground-motion simulation in a wave-field diffusive regime: Case study of the Mt. Vesuvius volcanic area. *Bulletin of the Seismological Society of America*, 98(3), 1272–1288.

Gok, E., and Polat, O. (2011). An assessment of the seismicity of the bursa region from a temporary seismic network. *Pure and Applied Geophysics*, 169(4), 659–675.

Gurenko, E. (2006). Earthquake Insurance in turkey: History of the turkish catastrophe Insurance Pool. World Bank Publications.

Gurpinar, A., Abalı, M., Yucemen, M. S., and Yesilcay, Y. (1978). Feasibility of mandatory earthquake insurance in Turkey. Earthquake Engineering Research Center, Report, (78-05).

Hashash, Y.M.A., Musgrove, M.I., Harmon, J.A., Groholski, D.R., Phillips, C.A., and Park, D. (2015) "DEEPSOIL 6.1, User Manual". Urbana, IL, Board of Trustees of University of Illinois at Urbana-Champaign

Hanks, T. C. (1979). Estimation of High-Frequency Strong Ground Motion. Journal of Geophysical Research, 84, 2235–2242.

Hanks, T. C. (1982). F\_Max. Bulletin of the Seismological Society of America, 72(6), 1867–1879.

Hanks, T. C., and Boore, D. M. (1984). Moment-magnitude relations in theory and practice. Journal of Geophysical Research, 89(B7), 6229.

Hanks, T. C., and McGuire, R. K. (1981). The character of high-frequency strong ground motion. Bulletin of the Seismological Society of America, 71 (6 ), 2071–2095.

Hartzell, S. H. (1978). Earthquake aftershocks as Green's functions. Geophysical Research Letters, 5(1), 1.

Haskell, N. A. (1964). Total energy and energy spectral density of elastic wave radiation from propagating faults. Bulletin of the Seismological Society of America, 54(6), 1811–1841.

Herrmann, R. B. (1985). An extension of random vibration theory estimates of strong ground motion to large distances. Bulletin of the Seismological Society of America, 75(5), 1447–1453.

Horasan, G., Ayse, K., Aysun, B., and Niyazi, T. (1998). S-wave attenuation in the Marmara Region, northwestern Turkey. Geophysical Research Letters, 25(14), 2733.

Housner, G. W. (1947). Characteristics of strong-motion earthquakes. Bulletin of the Seismological Society of America, 37(1), 19–31.

Housner, G. W. (1955). Properties of strong ground motion earthquakes. Bulletin of the Seismological Society of America, 45(3), 197–218.

Kaas, R., Goovaerts, M., Dhaene, J., and Denuit, M. (2008). *Modern actuarial risk theory: using R* (Vol. 128). Springer Science & Business Media.

Kanda, J., and Nishijima, K. (2004). Scope of insurance premium for residential houses against seismic risk in Japan. In *IFED forum* (pp. 5–9).

Kramer, S. L. (1996). *Geotechnical Earthquake Engineering*. Engineering (Vol. 6). Prentice Hall Upper Saddle River, NJ.

MATLAB, The MathWorks, Inc., Natick, Massachusetts, United States.

Mohammadioun, B., and Serva, L. (2001). Stress Drop , Slip Type , Earthquake Magnitude , and Seismic Hazard. *Bulletin of the Seismological Society of America*, 91(August), 694–707.

Motazedian, D., and Atkinson, G. M. (2005). Stochastic finite-fault modeling based on a dynamic corner frequency. *Bulletin of the Seismological Society of America*, 95(3), 995–1010.

Motazedian, D., and Moinfar, A. (2006). Hybrid stochastic finite fault modeling of 2003, M6.5, Bam earthquake (Iran). *Journal of Seismology*, 10(1), 91–103.

Nakamura, Y. (1989). A method for dynamic characteristics estimation of subsurface using microtremors on the ground surface. *Quarterly Report of the Railway Technical Research Institute*, 30(1), 25–33.

Ozturk N. Y. (2008). *Probabilistic Seismic Hazard Analysis: A Sensitivity Study With Respect To Different Models*. Unpublished, PhD Thesis, METU

Panzer, F., Rigano, R., Lombardo, G., Cara, F., Di Giulio, G., and Rovelli, A. (2011). The role of alternating outcrops of sediments and basaltic lavas on seismic urban scenario: the study case of Catania, Italy. *Bulletin of Earthquake Engineering*, 9(2), 411–439.

Papageorgiou, A. S., and Aki, K. (1983). A specific barrier model for the quantitative description of inhomogeneous faulting and the prediction of strong ground motion. I. Description of the model. *Bulletin of the Seismological Society of America*, 73(3), 693–722.

Paudel, Y., Botzen, W. J. W., and Aerts, J. (2013). Estimation of insurance premiums for coverage against natural disaster risk: an application of Bayesian Inference. *Natural Hazards and Earth System Science*, 13(3), 737–754.

Pitarka, A., Irikura, K., Iwata, T., and Sekiguchi, H. (1998). Three-dimensional simulation of the near-fault ground motion for the 1995 Hyogo-ken Nanbu (Kobe),

Japan, earthquake. *Bulletin of the Seismological Society of America*, 88(2), 428–440.

Raghukanth, S. T. G., and Somala, S. N. (2009). Modeling of strong-motion data in Northeastern India: Q, stress drop, and site amplification. *Bulletin of the Seismological Society of America*, 99(2 A), 705–725.

Rodolfo Saragoni, G., and Hart, G. C. (1973). Simulation of artificial earthquakes. *Earthquake Engineering & Structural Dynamics*, 2(3), 249–267.

Roumelioti, Z., Kiratzi, A., and Theodulidis, N. (2004). Stochastic strong ground-motion simulation of the 7 September 1999 Athens (Greece) earthquake. *Bulletin of the Seismological Society of America*, 94(3), 1036–1052.

Sanchez-Sesma, F. J. (1987). Site effects on strong ground motion. *Soil Dynamics and Earthquake Engineering*, 6(2), 124–132.

Schnabel, B., Schnabel, B., Lysmer, J., Lysmer, J., Seed, H. B., and Seed, H. B. (1972). SHAKE, A Computer program for earthquake response analysis of horizontally layered sites (EERC-72-12). EERC Report, 114.

Seed, R. B., Dickenson, S. E., and Idriss, I. M. (1991). Principal geotechnical aspects of the 1989 Loma Prieta earthquake. *Soils and Foundations*, 31(1), 1–26.

Shoja-Taheri, J., and Ghofrani, H. (2007). Stochastic finite-fault modeling of strong ground motions from the 26 December 2003 Bam, Iran, earthquake. *Bulletin of the Seismological Society of America*, 97(6), 1950–1959.

Silva, W., and Lee, K. (1987). WES RASCALS code for synthesizing earthquake ground motions. Department of the Army, US Army Corps of Engineers.

Thomson, W. T. (1959). Spectral aspect of earthquakes. *Bulletin of the Seismological Society of America*, 49(January), 91–98.

Topal, T., Doyuran, V., Karahanoglu, N., Toprak, V., Suzen, M. L., and Yesilnacar, E. (2003). Microzonation for earthquake hazards: Yenişehir settlement, Bursa, Turkey. *Engineering Geology*, 70(1), 93–108.

Toro, G. R., and McGuire, R. K. (1987). An investigation into earthquake ground motion characteristics in eastern North America. *Bull. Seism. Soc. Am.*, 77(2), 468–489.

Ugurhan, B., and Askan, A. (2010). Stochastic strong ground motion simulation of the 12 November 1999 Duzce (Turkey) earthquake using a dynamic Corner frequency approach. *Bulletin of the Seismological Society of America*, 100(4), 1498–1512.

Ugurhan, B., Askan, A., Akinci, A., and Malagnini, L. (2012). Strong-ground-motion simulation of the 6 April 2009 L'Aquila, Italy, earthquake. *Bulletin of the Seismological Society of America*, 102(4), 1429–1445.

Wells, D. L., and Coppersmith, K. J. (1994). New Empirical Relationships among Magnitude, Rupture Length, Rupture Width, Rupture Area, and Surface Displacement. *Bulletin of the Seismological Society of America*, 84(4), 974–1002.

Yalcinkaya, E. (2005). Stochastic finite-fault modeling of ground motions from the June 27, 1998 Adana-Ceyhan earthquake. *Earth, Planets and Space*, 57(2), 107–115.

Yaltirak, C. (2002). Tectonic evolution of the Marmara Sea and its surroundings. *Marine Geology*, 190(1-2), 493–529.

Yucemen, M. S. (2005). Probabilistic assessment of earthquake insurance rates for Turkey. *Natural Hazards*, 35(2), 291–313.

Zengin, E., and Cakti, E. (2014). Ground motion simulations for the 23 October 2011 Van, Eastern Turkey earthquake using stochastic finite fault approach. *Bulletin of Earthquake Engineering*, 12(2), 627–646.

SwissRe (2015). Swiss Reinsurance. [http://www.swissre.com/about\\_us/global\\_partnerships/Ramping\\_up\\_earthquake\\_resilience\\_in\\_Istanbul.html](http://www.swissre.com/about_us/global_partnerships/Ramping_up_earthquake_resilience_in_Istanbul.html). Last visited on November 2015.

TCIP (2015). Turkish Catastrophe Insurance Pool. <http://www.tcip.gov.tr/zorunlu-deprem-sigortasi-istatistikler.html>. Last visited on November 2015.



## APPENDIX A

### $\kappa_0$ VALUES FOR BURSA STATIONS

Table A.1  $\kappa_0$  Values for Bursa Stations

STATIONS	Kappa		R <sup>2</sup>	
	horizontal	vertical	horizontal	vertical
1601	0.0574	0.0557	0.7624	0.2051
1602	0.0125	0.0158	0.9551	0.9777
1603	0.0228	0.0177	0.7078	0.6546
1604	0.0589	0.0569	0.4344	0.2728
1605	0.0487	0.0270	0.7075	0.5004
1606	0.0616	0.0335	0.1925	0.3782
1607	0.0643	0.0498	0.6693	0.1123
1608	0.0572	0.0172	0.4583	0.5809
1609	0.0341	0.0168	0.7731	0.6987
1610	0.0649	0.0417	0.2591	0.4639
1611	0.0166	0.0059	0.5180	0.8671
1612	0.0779	0.0560	0.0345	0.0481
1613	0.0243	0.0100	0.6709	0.5105
1614	0.0387	0.0161	0.2470	0.4544
1615	0.0367	0.0170	0.8972	0.8561
1616	0.0507	0.0358	0.3702	0.1303
1617	0.0075	0.0184	0.9080	0.7957
1618	0.0331	0.0278	0.4328	0.4828
1619	0.0288	0.0118	0.8141	0.8281
1620	0.0200	0.0140	0.4223	0.4625
1621	0.0125	0.0136	0.4742	0.6530
1624	0.0192	0.0306	0.6619	0.8333
1625	0.0352	0.0391	0.2574	0.2707
1626	0.0366	0.0412	1.0000	1.0000
1627	0.0229	0.0261	0.7059	0.3267
1628	0.0349	0.0178	0.5239	0.5150
1629	0.0328	0.0159	0.6965	0.6845
1630	0.0506	0.0312	0.3959	0.5227
1631	0.0196	0.0213	0.4158	0.3931
1632	0.0177	0.0109	0.6981	0.5083
1633	0.0168	0.0137	0.3966	0.3372





Sondaj Derinliği Borehole Depth	Yeraltı Sıvısı Seviyesi Undergroundwater	Numune Derinliği Sample Depth	Numune Türü Sample Type	Standart Penetrasyon Densiyi Standard Penetration Test	Standart Penetrasyon Grafığı Standard Penetration Graph	Serbest Basınç Dayanımı / UCS	Zemin Sınıfı / Soil Classification	Zemin-Kaya Profili Soil-Rock Symbol	Zemin-Kaya Tanımlaması Soil-Rock Description	Plastisite İndisi / Plasticity Index	Doğal Su İçeriği / Natural Water	< 200 no.lu eliek < Sieve #200	Karot Yüzdesi Core Recovery	RQD
(m)	(m)	(m)		15 30 45	10 20 30 40 50	kPa	USCS			PI	W <sub>N</sub>	%	%	%
-11														
-12		12,00/12,45	SPT-8	13 20 26			SW-SM		Kahverengi - Yer Yer Gri, Siltli, (Çakılı) KUM, Yer Yer Kumlu ÇAKIL; Orta Sıkı - Çok Sıkı (Çakıl içeriği ardalanmalı azalıp artarak, % 0 - 52 arasında değişmektedir)	NP		9		
-13		13,50/13,95	SPT-9	13 8 13			SM			NP		22		
-14		15,00/15,45	SPT-10	17 30 35			SM			NP		14		
-15		16,50/16,95	SPT-11	21 41 42			SM		Brown - Locally Gray, Silty, (Gravelly) SAND, Locally Sandy GRAVEL; Medium Dense - Very Dense (Gravel content fluctuates between 0 and 52 %)	NP		16		
-16		18,00/18,45	SPT-12	16 21 27			SM			NP		14		
-17		19,50/19,95	SPT-13	18 22 36			SM			NP		21		
-18		21,00/21,45	SPT-14	18 20 22			SM			NP		18		
-19		22,50/22,95	SPT-15	15 18 23			SM			NP		15		
-20		24,00/24,45	SPT-16	15 15 20			SM			NP		18		
-21		25,50/25,95	SPT-17	17 19 22			SM		Brown, Silty SAND; Dense - Very Dense	NP		16		
-22		27,00/27,45	SPT-18	16 20 22			SM			NP		16		
-23		28,50/28,95	SPT-19	20 22 25			SM			NP		23		
-24		30,00/30,45	SPT-20	19 23 30			SM			NP		20		
-25														
-26														
-27														
-28														
-29														
-30									30,45 Kuru Sonu / End of Borehole	NP		20		

Figure B.2 Borehole log of station 1610 part 2

Sondaj Derinliği Borehole Depth	Yeraltısuyu Seviyesi Groundwater Level	Numune Derinliği Sample Depth	Numune Türü Sample Type	Standart Penetrasyon Deneyi Standard Penetration Test	Standart Penetrasyon Grafiği Standard Penetration Graph	Serbest Basınç Dayanımı / UCS	Zemin Sınıfı / Soil Classification	Zemin-Kaya Profili Soil-Rock Symbol	Zemin-Kaya Tanımlaması Soil-Rock Description	Plastisite İndisi / Plasticity Index	Doğal Su İçeriği / Natural Water	< 200 no.lu tük < Sieve #200	Karot Yüzdesi Core Recovery	RCQD
(m)	(m)	(m)		15 30 45	10 20 30 40 50	kPa	USCS			PI	W <sub>N</sub>	%	%	%
-1		1,50/1,95	SPT-1	5 7 6			SC		YAPAY DOLGU (Kahverengi - Koyu Kahverengi, Yer Yer Bloku, Kremit ve Tuğla Kanıtlan İçeren Çakılı, Kılı / Siltli Kum)	13		36		
-2														
-3		3,00/3,45	SPT-2	4 2 5			SM		ARTIFICIAL FILL (Brown - Dark Brown, Gravelly, Silty / Clayey Sand, Containing Pieces of Brick, etc., and Some Boulders)			28		
-4														
-5	4,80	4,50/4,53	SPT-3	50/3	(Boş / Empty)									
-5		4,50/5,50	K1											
-6		6,00/6,45	SPT-4	2 7 4			SP-SM		Açık Kahverengi, Az Siltli KUM, Orta Sıkı Light Brown, Slightly SAND, Medium Dense			10		
-7														
-8		7,50/7,95	SPT-5	4 5 7			CL		Kahverengi, Yeşilimsi Kahverengi, Kumlu KİL; Katı - Çok Katı / Kılı KUM; Orta Sıkı	20		63		
-9		8,50/9,00	UD-1				194 CL			17	20	71		
-9		9,00/9,45	SPT-6	7 10 12			SC		Brown - Greenish Brown, Sandy CLAY; Stiff - Very Stiff / Clayey SAND; Medium Dense	16		49		
-10														
-10		10,50/10,95	SPT-7	9 11 11			SP-SM		Krem - Açık Kahverengi, Yer Yer Az Çakılı Az Kumlu KİL; Çok Katı			6		

Figure B.3 Borehole log of station 1611 part 1

Sondaj Derinliği Borehole Depth	Yeraltısuyu Seviyesi Undergroundwater	Numune Derinliği Sample Depth	Numune Türü Sample Type	Standart Penetrasyon Deneji Standard Penetration Test	Standart Penetrasyon Grafiği Standard Penetration Graph	Serbest Basınç Dayanımı / UCS Zemin Sınıfı / Soil Classification	Zemin-Kaya Profili Soil-Rock Symbol	Zemin-Kaya Tanımlaması Soil-Rock Description	Plastisite İndisi / Plasticity Index	Doğal Su İçeriği / Natural Water	< 200 no.lu elek < Sieve #200	Karot Yüzdesi Core Recovery	RQD
(m)	(m)	(m)		15 30 45	10 20 30 40 50	kPa USCS			PI	W <sub>N</sub>	%	%	%
-11													
-12		12,00/12,45	SPT-8	12 12 14		SM	○	Krem - Açık Kahverengi, Yer Yer Çok Az Çakıllı, Az Siltli - Siltli KUM; Orta Sıkı	NP		16		
-13		13,50/13,95	SPT-9	10 10 18		SP-SM	○	Cream - Light Brown, Locally Very Slightly Gravelly, Slightly Siltly - Siltly SAND; Medium Dense	NP		6		
-14													
-15		15,00/15,45	SPT-10	10 11 11		ML		14.80 Koyu Gri, Kumlu SİLT, Çok Katı Dark Gray, Sandy SILT, Very Stiff	NP		51		
-16		16,50/16,95	SPT-11	4 4 3		CL		16.00		8	73		
-17		17,50/18,00	UD-2			69	CL	Gri - Koyu Gri KİL; Orta Katı	17	37	96		
-18		18,00/18,45	SPT-12	2 3 4			CL		18		95		
-19		19,00/19,50	UD-3			53	CL	Gray - Dark Gray CLAY; Medium Stiff	19	37	100		
-20		19,50/19,95	SPT-13	2 3 3			CL		18		94		
-21		20,40/21,00	UD-4	(Alınmadı / Not Recovered)			CL-ML		4		95		
-22		21,00/21,45	SPT-14	2 2 3				21.50					
-23		22,00/22,50	UD-5	(Alınmadı / Not Recovered)			ML		NP		54		
-24		22,50/22,95	SPT-15	2 4 27									
-25		24,00/24,45	SPT-16	8 6 8		SM	○	Koyu Gri, Yer Yer Çok Az Çakıllı, Siltli İnce KUM; Orta Sıkı / Kumlu SİLT; Katı - Çok Katı	NP		36		
-26		25,50/25,95	SPT-17	8 11 13		ML		Dark Gray, Locally Very Slightly Gravelly, Siltly Fine SAND; Medium Dense / Sandy SILT; Stiff - Very Stiff	NP		55		
-27		27,00/27,45	SPT-18	6 7 6		SM	○	27.50		NP	37		
-28		28,00/28,50	UD-6			68	CL		17	37	58		
-29		28,50/28,95	SPT-19	6 8 8			CL-ML	Koyu Gri, Yer Yer Kumlu KİL / SİLT; Katı - Çok Katı	5		62		
-30		30,00/30,45	SPT-20	7 8 8			CL-ML	Dark Gray, Locally Sandy CLAY / SİLT; Stiff - Very Stiff	3		82		

Figure B.4 Borehole log of station 1611 part 2

Sondaj Derinliği Borehole Depth (m)	Yeraltısuyu Seviyesi Undergroundwater (m)	Numune Derinliği Sample Depth (m)	Numune Türü Sample Type	Standart Penetrasyon Deneyi Standard Penetration Test			Standart Penetrasyon Grafiği Standard Penetration Graph					Serbest Basınç Dayanımı / LCS kPa	Zemin Sınıfı / Soil Classification USCS	Zemin-Kaya Profili Soil-Rock Symbol	Zemin-Kaya Tanımlaması Soil-Rock Description	Plastisite İndisi / Plasticity Index PI	Doğal Su İçeriği / Natural Water W <sub>N</sub>	<200 no.lu elek < Sieve #200 %	Karat Yüzdesi Core Recovery %	RQD %
				15	30	45	10	20	30	40	50									
-31		31,00/31,50	UD-7	(Alınmadı)																
		31,50/31,95	SPT-21		7	7	9						ML					86		
-32																				
		33,00/33,45	SPT-22		8	8	8						CL		Koyu Gri, Yer Yer Kumlu KİL / SILT; Katı - Çok Katı	9		97		
-34		34,00/34,50	UD-8									75	CL		Dark Gray, Locally Sandy CLAY / SILT; Stiff - Very	17	32	97		
		34,50/34,95	SPT-23		3	5	7						CL-ML		Stiff	7		87		
-36		36,00/36,45	SPT-24		2	4	6						ML					70		
-37																				
		37,50/37,95	SPT-25		13	15	25						SM		37.00 Siyah - Siyahimsi Koyu Gri, Az Siltli İnce KUM, Sıkı - Çok Sıkı			12		
-38															Black - Dark Blackish Gray, Slightly Silty Fine SAND, Dense - Very Dense					
		39,00/39,45	SPT-26		19	24	28						SP-SM		39.45 Kuyu Sonu / End of Borehole			8		

Figure B.5 Borehole log of station 1611 part 3

Sondaj Derinliği Borehole Depth (m)	Artezyen Artesian	Yeraltısuyu Seviyesi Groundwater Level (m)	Numune Derinliği Sample Depth (m)	Numune Türü Sample Type	Standart Penetrasyon Deneyi Standard Penetration Test			Standart Penetrasyon Grafiği Standard Penetration Graph					Serbest Basınç Dayanımı / LCS kPa	Zemin Sınıfı / Soil Classification USCS	Zemin-Kaya Profili Soil-Rock Symbol	Zemin-Kaya Tanımlaması Soil-Rock Description	Plastisite İndisi / Plasticity Index PI	Doğal Su İçeriği / Natural Water W <sub>N</sub>	<200 no.lu elek < Sieve #200 %	Karat Yüzdesi Core Recovery %	RQD %
					15	30	45	10	20	30	40	50									
-1																					
			1,50/1,95	SPT-1	1	1	1							SM		BITKİSEL TOPRAK / TOPSOIL 0.20			18		
-3			3,00/3,45	SPT-2	2	4	5							SM		Koyu Gri, Siltli, Yer Yer Çalkılı Kaba KUM, Çok Gevşek - Sıkı			24		
-5			4,50/4,95	SPT-3	15	17	18							SP-SM		Dark Gray, Silty, Locally Gravelly Coarse SAND; Very Loose - Dense			10		
-6			6,00/6,45	SPT-4	3	13	19							SM					15		
-8			7,50/7,95	SPT-5	8	10	13							ML		7.00 Koyu Yeşilimsi Gri, Kumlu SİLT, Çok Katı / Siltli KUM; Orta Sıkı			55		
-9			9,00/9,45	SPT-6	5	9	11							SM		Dark Greenish Gray, Sandy SILT, Very Stiff / Silty SAND; Medium Dense			48		
-10			10,50/10,95	SPT-7	3	5	7							SM					33		

Figure B.6 Borehole log of station 1612 part 1

Sondaj Derinliği Borehole Depth	Yeraltısuyu Seviyesi Undergroundwater	Numune Derinliği Sample Depth	Numune Türü Sample Type	Standart Penetrasyon Deneği Standard Penetration Test	Standart Penetrasyon Grafiği Standard Penetration Graph	Serbest Basınç Dayanımı / LCS Zemin Sınıfı / Soil Classification	Zemin-Kaya Profili Soil-Rock Symbol	Zemin-Kaya Tanımlaması Soil-Rock Description	Plastisite İndisi / Plasticity Index	Doğal Su İçeriği / Natural Water	<200 no. tanelek % Sieve #200	Karot Yüzdesi Core Recovery	RQD
(m)	(m)	(m)		15 30 45	10 20 30 40 50	kPa USCS			PI	W <sub>N</sub>	%	%	%
-11								Koyu Yeşilimsi Gri, Siltli KUM; Orta Sıkı Dark Greenish Gray, Silty SAND; Medium Dense 11.50					
-12		12,00/12,45	SPT-8	3 4 3	●	CL			NP		82		
-13		13,00/13,50	UD-1			60 CL			12	30	99		
-13		13,50/13,95	SPT-9	2 3 2	●	SC			23		35		
-14		14,50/15,00	UD-2			21 CL-ML			7	34	88		
-15		15,00/15,45	SPT-10	2 4 2	●	ML	Koyu Gri, Yer Yer Az Kumlu KİL; Çok Yumuşak - Orta Katı	6					
-16		16,00/16,50	UD-3			44 CL	(13,50 - 14,50 m arası killi kum; 14,50 - 19,00 m arası silt - çok düşük plastisiteli kil)	16	43	99			
-16		16,50/16,95	SPT-11	2 2 1	●	ML		12					
-17		17,50/18,00	UD-4	(Alınmadı / Not Recovered)									
-18		18,00/18,45	SPT-12	1 2 2	●	ML		14					
-19		19,00/19,50	UD-5			23 CL		21	48	98			
-19		19,50/19,95	SPT-13	1 2 3	●	CL		26					
-20		20,50/21,00	UD-6			43 CL		17	49	99			
-21		21,00/21,45	SPT-14	1 0 1	●	CL		27		98			
-22		22,00/22,50	UD-7	(Alınmadı / Not Recovered)									
-22		22,50/22,95	SPT-15	0 0 1	●	CL		25		97			
-23		23,50/24,00	UD-8	(Alınmadı / Not Recovered)									
-24		24,00/24,45	SPT-16	1 1 1	●	CL		25		99			
-25		25,00/25,50	UD-9	(Alınmadı / Not Recovered)									
-25		25,50/25,95	SPT-17	1 2 1	●	CL	Dark Gray, Locally Slightly Sandy CLAY; Very Soft - Medium Stiff	26		94			
-26		26,50/27,00	UD-10	(Alınmadı / Not Recovered)			(Clayey sand from 13,50 to 14,50 m depth, silt - clay of very low plasticity from 14,50 to 19,00 m depth.)	21					
-27		27,00/27,45	SPT-18	1 1 1	●	CL							
-28		28,00/28,50	UD-11			59 CL		23	59	99			
-28		28,50/28,95	SPT-19	2 2 3	●	CL		26					
-29		29,50/30,00	UD-12	(Alınmadı / Not Recovered)									
-30		30,00/30,45	SPT-20	2 2 1	●	CH		30		97			

Figure B.7 Borehole log of station 1612 part 2

Sondaj Derinliđi Borehole Depth	Yeraltısuyu Seviyesi Undergroundwater	Numune Derinliđi Sample Depth	Numune Türü Sample Type	Standart Penetrasyon Deneyi Standard Penetration Test	Standart Penetrasyon Grafiđi Standard Penetration Graph	Serbest Basıncı Dayanımı / UCS	Zemin Sınıfı / Soil Classification	Zemin-Kaya Profili Soil-Rock Symbol	Zemin-Kaya Tanımlaması Soil-Rock Description	Plastisite İndisi / Plasticity Index	Dođal Su İceriđi / Natural Water	< 200 no.lu eiek < Sieve #200	Kararlı Yüzdesi Core Recovery	RQD
(m)	(m)	(m)		15 30 45	10 20 30 40 50	kPa	USCS			PI	W <sub>n</sub>	%	%	%
-31		31,00/31,50	UD-13	(Alınmadı)	Not Recovered				Koyu Gri KİL, Çok Yumuşak- Orta Katı					
		31,50/31,95	SPT-21	0 1 1			CL			26		83		
-32		32,50/33,00	UD-14	(Alınmadı)	Not Recovered				Koyu Siyahımsı Gri, Az Kumlu KİL, Çok Yumuşak					
-33		33,00/33,45	SPT-22	0 0 1			CH			31		88		
-34		34,00/34,50	UD-15	(Alınmadı)	Not Recovered				Dark Blackish Gray, Slightly Sandy CLAY; Very Soft					
-35		34,50/34,95	SPT-23	0 1 1			CH			31		88		
-36		35,50/36,00	UD-16	(Alınmadı)	Not Recovered									
-36		36,00/36,45	SPT-24	1 1 1			CL			32		93		
-37		37,50/37,95	SPT-25	13 25 27			SM			NP		13		
-38		39,00/39,45	SPT-26	18 26 35	(Boş / Empty)				Koyu Siyahımsı Gri, Siltli, İnce KUM; Çok Sıkı					
-39		40,50/40,77	SPT-27	26 50/12			SM		Dark Blackish Gray, Silty, Fine SAND; Very Dense					
-40														
-41									40,77 Kuru Sonu / End of Borehole	NP		49		

Figure B.8 Borehole log of station 1612 part 3

Sondaj Derinliđi Borehole Depth	Yeraltısuyu Seviyesi Groundwater Level	Numune Derinliđi Sample Depth	Numune Türü Sample Type	Standart Penetrasyon Deneyi Standard Penetration Test	Standart Penetrasyon Grafiđi Standard Penetration Graph	Serbest Basıncı Dayanımı / UCS	Zemin Sınıfı / Soil Classification	Zemin-Kaya Profili Soil-Rock Symbol	Zemin-Kaya Tanımlaması Soil-Rock Description	Plastisite İndisi / Plasticity Index	Dođal Su İceriđi / Natural Water	< 200 no.lu eiek < Sieve #200	Kararlı Yüzdesi Core Recovery	RQD
(m)	(m)	(m)		15 30 45	10 20 30 40 50	kPa	USCS			PI	W <sub>n</sub>	%	%	%
-1		1,50/1,95	SPT-1	8 16 12			SM		Koyu Kahverengi, Az Çakıllı, Siltli KUM; Orta Sıkı					
									Dark Brown, Slightly Gravelly, Silty SAND; Medium Dense	NP		26		
-2									1,80					
-3		3,00/3,45	SPT-2	8 13 15			SP		Krem - Açık Kahverengi, İnce KUM; Orta Sıkı					
									Cream - Light Brown, Fine SAND; Medium Dense			2		
-4		4,50/4,95	SPT-3	4 4 5			CL			25		78		
-5	Yok None	5,00/5,50	UD1				CL		Koyu Kahverengi, Az Çakıllı, Kumlu - Çok Kumlu	24	31	81		
									KİL, Katı - Çok Katı					
-6		6,00/6,45	SPT-4	5 9 9			CL		Dark Brown, Slightly Gravelly, Sandy - Very Sandy	15		64		
									CLAY; Stiff - Very Stiff					
-7		7,50/7,76	SPT-5	27 50/11					7,50					
-8									Krem - Açık Kahverengi, Yer Yer Açık Yeşil, Orta					
									Çatlaklı, Orta - Çok Ayrışmış; MARN; Çok Zayıf - Zayıf					
-9		9,00/9,13	SPT-6	50/13										
									Cream - Light Brown, Locally Light Green, Moderately					
-10		9,50/11,00	K1						Jointed, Moderately - Highly Weathered MARL; Very					
									Weak - Weak			80	19	

Figure B.9 Borehole log of station 1614 part 1

Sondaj Derinliđi Borehole Depth	Yeraltısuyu Seviyesi Undergroundwater	Numune Derinliđi Sample Depth	Numune Türü Sample Type	Standart Penetrasyon Deneyi Standard Penetration Test	Standart Penetrasyon Grafiđi Standard Penetration Graph	Serbest Basıncı Diyametri / UCS	Zemin Sınıfı / Soil Classification	Zemin-Kaya Profili Soil-Rock Symbol	Zemin-Kaya Tanımlaması Soil-Rock Description	Plastisite İndisi / Plasticity Index	Dođal Su İceriđi / Natural Water	< 200 no.lu elek % Sieve #200	Karot Yüzdesi Core Recovery	RQD
(m)	(m)	(m)		15 30 45	10 20 30 40 50	kPa	USCS			PI	W <sub>n</sub>	%	%	%
-11		9.50/11.00	K1						Krem - Açık Kahverengi, Yer Yer Açık Yeşil, Orta Çatalıklı, Orta - Çok Ayrışmış MARN, Çok Zayıf - Zayıf				80	19
-12		11.00/12.50	K2						Cream - Light Brown, Locally Light Green, Moderately Jointed, Moderately - Highly Weathered MARL, Very Weak - Weak				90	36
-12									12.50 Kuyu Sonu / End of Borehole					

Figure B.10 Borehole log of station 1614 part 2

## APPENDIX C

### CORRELATIONS OF SEISMIC VELOCITIES WITH GEOTECHNICAL BOREHOLE DATA AT STATIONS 1610, 1611, 1612 AND 1614

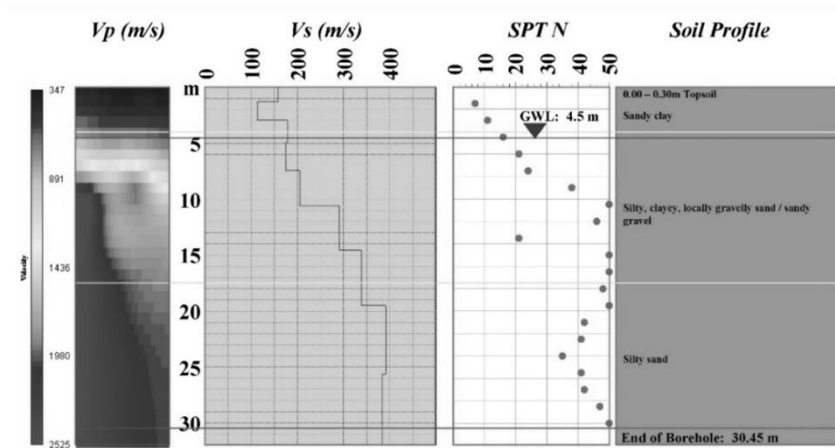


Figure C.2 Correlations of seismic velocities with geotechnical borehole data at station 1610

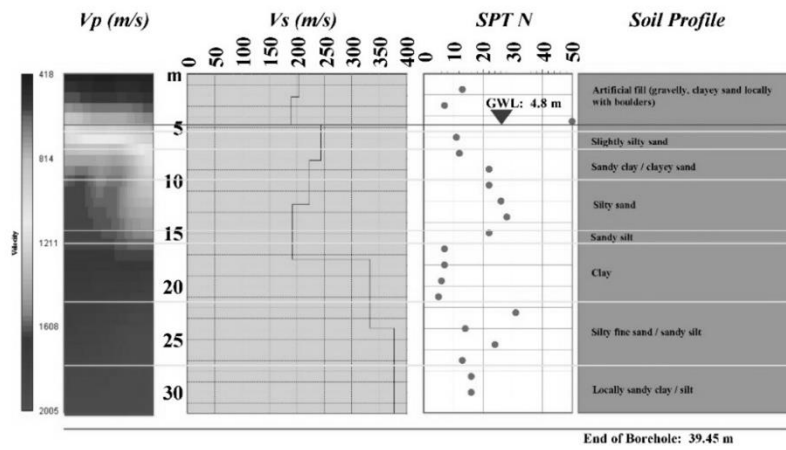


Figure C.2 Correlations of seismic velocities with geotechnical borehole data at station 1611

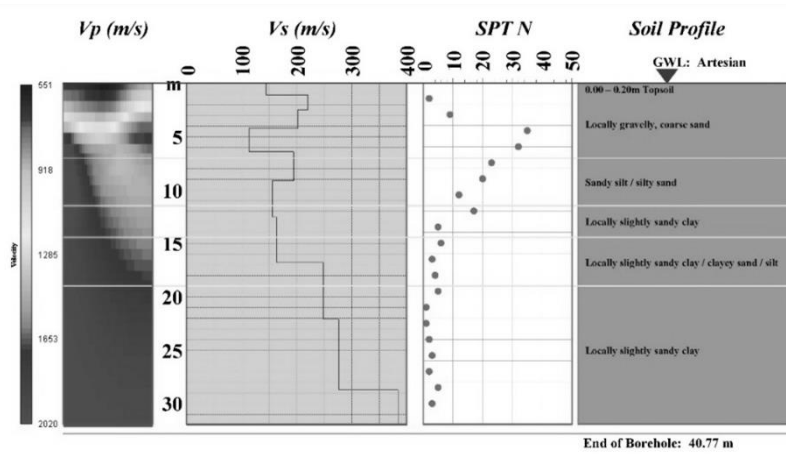


Figure C.3 Correlations of seismic velocities with geotechnical borehole data at station 1612

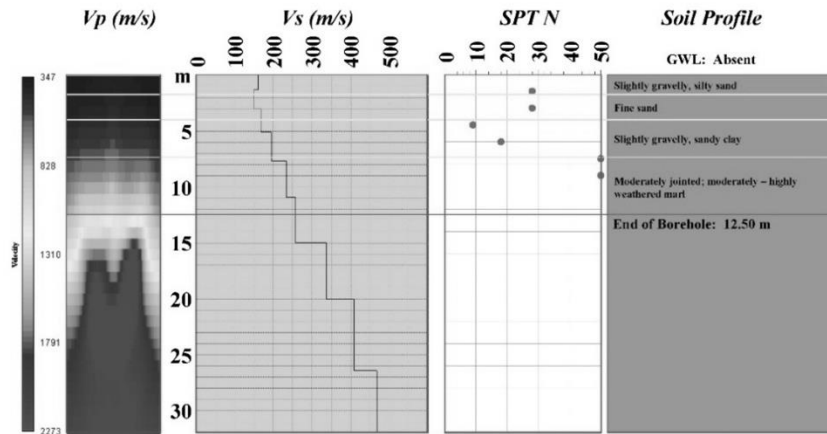


Figure C.4 Correlations of seismic velocities with geotechnical borehole data at station 1614